



# Mineralogy, Chemistry, and Thermal and Surface Properties of Various Technological Types of K-Bentonite from the Dolná Ves Deposit (Kremnické vrchy Mts., Western Carpathians, Slovakia)

M. Osacký · Y. Bai · P. Uhlík · H. Pálková · M. Čaplovičová

Accepted: 17 November 2023 / Published online: 8 December 2023  
© The Author(s) 2023

**Abstract** The Dolná Ves K-bentonite deposit is one of a few known economic accumulations of illite-smectite in the world. Several studies have been done on the illite-smectitic component isolated from the Dolná Ves K-bentonite, but there is a shortage of analytical data on the K-bentonite itself. The main goal of the present study was to perform mineralogical and physico-chemical characterizations of various technological types of K-bentonites from the Dolná Ves deposit to better understand the relationships between the various qualitative types and their properties. The type I (high-grade) K-bentonite contains 88–91 wt.%

of illite-smectite. The type II (low-grade) K-bentonite contained substantially less illite-smectite, ranging from 37 to 63 wt.%. The illite-smectites isolated from the type I K-bentonites displayed greater expandability, contained more octahedral Mg and less octahedral Fe, had greater cation exchange capacity (CEC), smaller thickness of fundamental particles, and thinner illite-smectite crystals in comparison with illite-smectites from the type II K-bentonites. The LOI (loss-on-ignition) and Al<sub>2</sub>O<sub>3</sub> content increased with increasing amount of illite-smectite. The increase in the expandability by 10% corresponded to an increase in CEC by ~10 meq/100 g. The type I K-bentonites had much greater mass loss at <250°C due to greater expandability. The best tilemaking performance was expected for the type I K-bentonite. This raw material could also be potentially valuable for the pharmaceutical, cosmetic and food industries. Overall, the results showed that the studied technological types of K-bentonites from the Dolná Ves deposit differ not only in terms of illite-smectite contents but also in terms of the nature of the illite-smectites.

Associate Editor: Michal Skiba

**Supplementary Information** The online version contains supplementary material available at <https://doi.org/10.1007/s42860-023-00262-4>.

M. Osacký (✉) · Y. Bai · P. Uhlík  
Department of Mineralogy, Petrology and Economic Geology, Comenius University in Bratislava, Mlynska Dolina, Ilkovicova 6, Bratislava 84215, Slovakia  
e-mail: mosacky@hotmail.com

H. Pálková  
Institute of Inorganic Chemistry, Slovak Academy of Sciences, Dúbravská Cesta 9, Bratislava 84536, Slovakia

M. Čaplovičová  
Centre for Nanodiagnosics of Materials, Faculty of Materials Science and Technology, Slovak University of Technology, Vazovova 5, Bratislava 81243, Slovakia

**Keywords** Dolná Ves · Illite-smectite · K-bentonite · Mineralogy · Slovakia

## Introduction

Although interstratified illite-smectite is one of the most abundant clay minerals in sedimentary rocks and soils, economic accumulations of illite-smectite are

rare and few K-bentonite deposits are mined around the world (e.g. Dolná Ves deposit, Kremnické vrchy Mts., Slovakia and Füzéradvány deposit, Tokaj Mts., Hungary). Bentonite is a clay rock formed by the alteration of volcanic glass, consisting predominantly of smectite minerals, usually montmorillonite. Smectite can be converted to interstratified illite-smectite through the addition of non-exchangeable potassium in the inter-layer position. The resulting clay rock rich in illite-smectite is called K-bentonite (Weaver, 1953). The mineable illite-smectite deposits are principally formed by the interaction of permeable rhyolitic rocks rich in volcanic glass (tuffs) with hydrothermal solutions having temperatures between 100 and 200°C, close to neutral pH and enriched in potassium (Pécskay et al., 2005; Šucha et al., 1992; Uhlík & Majzlan, 2004).

The structure of illite-smectite consists of two different components, i.e. expandable smectitic and non-expandable illitic layers. Illite-smectite can have an ordered (regular) or disordered (irregular) interstratified structure, depending on the periodic or random stacking of smectitic and illitic layers along the *c* direction (Reichweite parameter – R) (Jagodzinski, 1949). The expandability (S) is a parameter that expresses the percentage of smectitic interlayers within the interstratified illite-smectite structure. Illite-smectite is usually formed by illitization of smectite. Smectite-to-illite transformation via interstratified illite-smectite is commonly associated with burial diagenesis, low-grade metamorphism, and hydrothermal alteration (Hower et al., 1976; Inoue et al., 1978, 2005; Kraus et al., 1994). In the course of smectite illitization, the number of illitic layers increases with increasing temperature (e.g. Šucha et al., 1992). As a consequence, the ordering of layer stacking gradually changes from smectite-rich R0 illite-smectite to illite-rich R3 illite-smectite. Smectite-to-illite transformations and interstratifications between smectitic and illitic layers in illite-smectite have been studied intensively over the past several decades mainly due to their application in the oil industry for oil exploration (e.g. Drits et al., 1996, 1997; Inoue et al., 1978; Środoń, 1999).

In the present study, K-bentonites from the Dolná Ves deposit located in the southern part of the Kremnické vrchy Mountains in the Western Carpathians, were examined. The Dolná Ves deposit is classified as a ceramic clays deposit with the K-bentonite reserves of ~9 Mt (Zuberec et al., 2005). The deposit

is occasionally mined with the annual K-bentonite production up to 5000 tons (Šoltés et al., 2021). The thickness of the productive layer is ~10 m (locally up to 60 m). The principal use of K-bentonite from the Dolná Ves deposit is in the manufacture of ceramic floor and wall tiles. The addition of K-bentonite enhances the technological properties of ceramics. From a technological point of view, at least two types of raw materials can be distinguished at the Dolná Ves deposit (Hroncová et al., 1992; Šucha et al., 1992). Type I material is finer with a greater illite-smectite content; it is suitable for the ceramics industry without the need for processing. Type II material is coarser with a smaller illite-smectite content; this material needs to be processed prior to use in the ceramics industry. Type I is primarily concentrated in the central parts of the deposit while the type II is present in the marginal parts (Hroncová et al., 1992; Šucha et al., 1992).

The Dolná Ves deposit was formed by low-sulfidation hydrothermal alteration of smectitic clays which originated from rhyolitic tuffs (Kraus et al., 1994). Two types of illite-smectite interstratification (R1 and R3) and one polytype (1 *M*) were reported from the deposit (Šucha et al., 1992). The expandability of illite-smectites from Dolná Ves ranged between 6 and 45% (Šucha et al., 1992). The documented decrease in expandability from the south to the north at the Dolná Ves deposit was associated with the decrease in the temperature of hydrothermal solutions coming from the north (Šucha et al., 1992). The maximum temperature of hydrothermal solutions was estimated at 140–160°C (Uhlík & Majzlan, 2004).

Unusually large (*ab* dimensions), thin (*c* dimensions), and flexible crystals of illite-smectite were reported from the Dolná Ves deposit (Šucha et al., 1996). Illite-smectite particles of this type were probably responsible for discrepancies between the expandabilities obtained from high-resolution transmission electron microscopy (HRTEM) and XRD. The much greater expandabilities obtained by XRD are attributed to the intercrystal diffraction effect resulting from the ability of large and thin illite-smectite particles to build face-to-face contacts during the preparation of oriented specimens for XRD (Šucha et al., 1996). Another source of discrepancy (Dudek et al., 2002) between XRD and HRTEM is related to the underestimation of the contributions of thicker particles by HRTEM.

This underestimation comes from inaccurate counting statistics for thick crystals and the availability of number-weighted distributions, in contrast to the area-weighted distributions registered by XRD.

The dynamics and mechanism of structural transformations of hydrothermal illite-smectites from the Dolná Ves deposit were studied by Drits et al. (1996). They showed that the changes in physico-chemical conditions (increasing temperature and/or K concentration in the solution) led to a recrystallization of illite fundamental particles which was accompanied not only by an increase in the thickness of illite fundamental particles and a decrease in the proportion of smectite interlayers but also by a related increase in the amounts of 2:1 layers with *trans*-vacant octahedra in these illite fundamental particles. The investigation of illite-smectites of hydrothermal origin from the Dolná Ves deposit also contributed to a better understanding that the processes for the formation of illite-smectite minerals are not universal but depend on the origin of illite-smectite (e.g. hydrothermal alteration versus burial diagenesis, etc.) (Drits et al., 1996). In one of the more recent papers associated with the Dolná Ves deposit (Šucha et al., 2001), the contemporary weathering profile developed on the top surface of the Dolná Ves deposit was examined to study the processes of illite-smectite weathering under temperate climatic conditions.

The previous studies on the Dolná Ves deposit (e.g. Drits et al., 1996; Šucha et al., 1992, 1996) focused primarily on the investigation of illite-smectite-enriched size fractions (<2 and <1 μm) separated from the whole-rock K-bentonite. In the present study, different technological types of Dolná Ves K-bentonites were collected and both whole-rocks and various size fractions (>2000, 500–2000, 63–500, 2–63, <2, 0.2–2, and <0.2 μm) separated from the whole-rock samples were analyzed. The main differences in mineralogy, chemistry, and surface and thermal properties for the two technological types of K-bentonites are reported in the present study.

The main goal was to find and better understand the relationships between the various technological types of K-bentonites and their properties, which may result in various possible applications of K-bentonites from the Dolná Ves deposit. A further goal was to compare the results obtained in the present study with the data for the Special clay ISCz-1 (illite-smectite from the Dolná Ves deposit) which has been part of

the Source Clays Repository of The Clay Minerals Society Source Clays since the 1990s.

## Geological Settings

The Kremnické vrchy Mountains range is situated in the northern part of the Central Slovakia Volcanic Field. The volcanites include remnants of a large Neogene andesite stratovolcano with subvolcanic intrusive rocks in the central zone, a north–south trending graben with volcanic formations including differentiated rocks >1000 m thick and resurgent horst in the central part of the graben associated with the late-stage rhyolite magmatic activity (Lexa et al., 1998).

The Dolná Ves deposit (Fig. 1) is located in the southern part of the Kremnické vrchy Mountains (1.5 km west-southwest of Dolná Ves village and 2 km south of the elevation Čertov vrch) and belongs to the Jastrabá Formation (Fm.). The Jastrabá Fm. consists of rhyolitic volcanism products represented by volcanic extrusions, lava flows, tuffs, and epiclastics which form a continuous 100–300 m thick complex (Lexa et al., 1998, 2021). Rhyolites of the Jastrabá Fm. are associated with the back-arc extension of the Carpathian arc (Lexa & Konečný, 1998). The biostratigraphic data (high pollen content derived from the genera *Sequoia*, *Salix*, *Ilex*, and *Graminae*) suggest the Late Sarmatian to Early Pannonian age of the Jastrabá Fm. (Konečný et al., 1983). The results of radiometric dating of rhyolites by K–Ar, as well as Rb–Sr methods fall in the interval from  $12.2 \pm 0.3$  Ma to  $11.4 \pm 0.4$  Ma (Chernyshev et al., 1995, 2013; Lexa & Pécskay, 2010). Permeable rhyolite rocks of the Jastrabá Fm., rich in volcanic glass (volcanoclastics and perlites), were altered extensively into the economic accumulations of bentonites, K-bentonites, and zeolites (Kraus et al., 1994; Šamajová et al., 1992). The main alteration products in the southern part of the Jastrabá Fm. are composed mainly of smectite (montmorillonite), locally forming the bentonite deposits such as Stará Kremnička III, Stará Kremnička–Jeľšovský potok, Lutilla I, Lutilla–Pod Klapou, Bartošova Lehôtká, and Kopernica (e.g. Górnjak et al., 2016, 2017; Osacký et al., 2019).

The Dolná Ves K-bentonite deposit is located between the rhyolitic cryptodomes which were emplaced near the rhyolite volcanoclastic complex as shallow laccoliths. The cryptodomes in the apical and

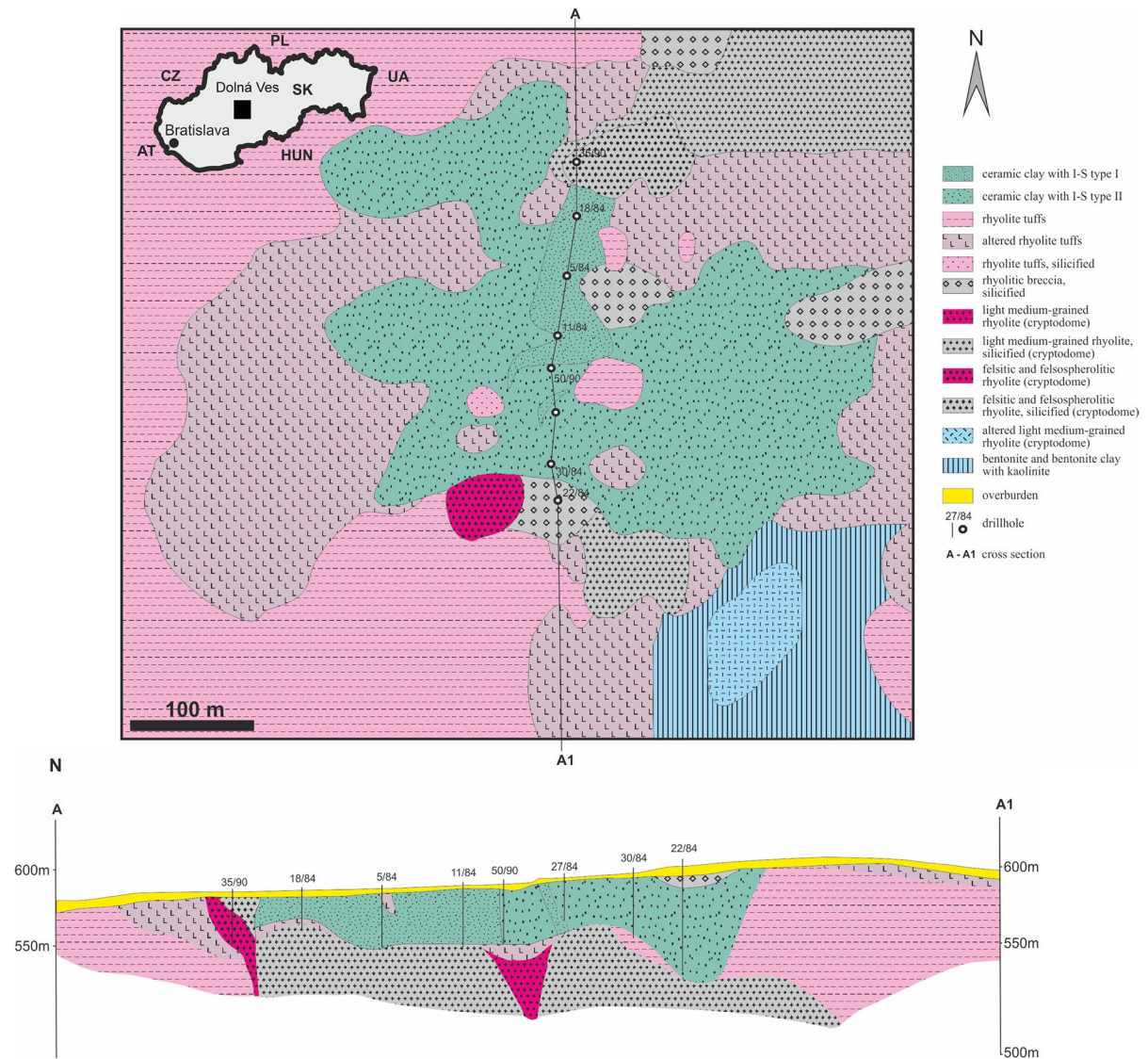


**Fig. 1** Geological map (upper) and cross section (lower) of the Dolná Ves deposit (modified from Hroncová et al., 1992)

marginal parts often pass into breccias. The cryptodome bodies are massive or slightly porous, formed by rhyolites with a characteristic spherulitic or felsitic structure. Macroscopically, they are predominantly light to white medium-grained rocks with sanidine. The sanidine rhyolites are the youngest rhyolites in the vicinity of the Dolná Ves deposit (Demko et al., 2010; Hroncová et al., 1992). The parent rocks for the K-bentonite at the Dolná Ves deposit were rhyolite volcanoclastics (pumice rhyolite tuffs and tuff breccias) and breccias of rhyolitic cryptodomes. The genesis of the Dolná Ves deposit is connected

with the low hydrothermal alteration processes. The source of hydrothermal fluids was associated with the Kremnica hydrothermal ore veins system. The subsurface flow of hydrothermal fluids through the permeable rocks was driven by a decreasing hydraulic head (from the north to the south), with local discharge on paleosurfaces (e.g. Čertov Vrch hot spring system). The major alterations observed at the Dolná Ves deposit were silicification and K-metasomatism. The hydrothermal genetic model proposed for the Dolná Ves deposit was supported by stable-isotope and fluid-inclusions studies and by the illite-smectite



expandability measurements, showing the expandability increase from the north to the south (Hroncová et al., 1992; Koděra et al., 2014; Kraus et al., 1994; Šucha et al., 1992; Uhlík & Majzlan, 2004).

## Materials and Methods

### Materials

Five samples: DV19/1, DV19/2, DV19/3, DV19/4, and DV19/5 collected at the Dolná Ves deposit in 2019 were used in the present study. The global positioning system (GPS) coordinates for sampling sites are reported in Table S1. The samples were dried for 48 h at 60°C. From dried solids, several size fractions were isolated by wet sieving (>2000, 500–2000, and 63–500 µm), settling (2–63 and <2 µm), and centrifugation (0.2–2 and <0.2 µm) in distilled water. Prior to size separation, the dried bulk solids were dispersed in distilled water by stirring for 24 h at room temperature. All separated fractions were dried overnight at 60°C, ground gently in an agate mortar, passed through a 250 µm sieve, and subsequently analyzed. The natural forms of the samples studied were used because no significant changes in the XRD patterns, XRD expandability, and CEC values were observed between the natural and Na-saturated forms of the <2 µm size fractions.

### Methods

X-ray diffraction patterns of oriented (air-dried and ethylene glycolated) and random preparations were recorded using a Phillips PW1710 diffractometer (Philips Analytical, Almelo, The Netherlands), with CuK $\alpha$  radiation and a graphite monochromator (20 mA and 35 kV). The oriented preparations were analyzed from 2 to 60°2 $\theta$  with a step size of 0.02°2 $\theta$  and a counting time of 0.08 s per step. The oriented preparations were made by dispersing ~130 mg of clay fraction (<2, 0.2–2, and <0.2 µm) in 2 mL of distilled water using an ultrasonic cleaner, Tesla UC 006 DM1 (Tesla, Vráble, Czechoslovakia) (3–5 min at 150 W), pipetting the suspension onto a glass slide, and drying at room temperature. The quantitative mineralogical composition was determined from XRD random preparations using *RockJock* software (Eberl, 2003). Samples for quantitative X-ray diffraction (QXRD)

analysis were prepared according to a method modified by Omotoso and Eberl (2009) from that reported by Środoń et al. (2001). The sample was passed through a 250 µm sieve. Then, 1 g of sample was mixed with 0.250 g of corundum (American Elements, Los Angeles, California, USA) and ground with 4 mL of ethanol (Centralchem, Bratislava, Slovakia) in a McCrone micronizing mill (McCrone Associates, Westmont, Illinois, USA) for 5 min. The dried (60°C overnight) sample/corundum mixture was then shaken in a plastic vial with three plastic balls using a Retsch MM 200 mill (Retsch, Haan, Germany). Hexane (Centralchem, Bratislava, Slovakia) was added to the mixture in the ratio of 0.5 mL hexane to 1 g of pure clay and the vial was shaken for an additional 10 min. The powder was passed through the 250 µm sieve again and side loaded into an XRD holder. Samples were X-rayed from 4 to 65°2 $\theta$  with a step size of 0.02°2 $\theta$  and a counting time of 2 s per step. The XRD intensities extracted from the XRD files using *Jade* software were entered into the *RockJock* program and the mineralogical composition was calculated.

The XRD expandability ( $S_{\text{XRD}}$ ) for the illite-smectites studied was calculated from ethylene glycol-solvated XRD patterns (<2, 0.2–2, and <0.2 µm fractions) using differential °2 $\theta$  measurements from the reflections near 17 and 26°2 $\theta$  (Dudek & Środoń, 1996), 44 and 46°2 $\theta$  (Środoń, 1980), and 9 and 17°2 $\theta$  (Moore & Reynolds, 1997). The  $S_{\text{XRD}}$  values reported are the average from the three expandabilities determined according to Dudek & Środoń (1996), Środoń (1980), and Moore and Reynolds (1997).

The illite-smectites from Na-saturated clay fractions (<2, 0.2–2, and <0.2 µm) were separated into fundamental illite particles by treatment with polyvinylpyrrolidone (PVP) (Sigma-Aldrich, Saint Louis, Missouri, USA) following the procedure reported by Eberl et al. (1998). The PVP-clay suspensions were sonified using an ultrasonic cleaner Tesla UC 006 DM1 (Tesla, Vráble, Czechoslovakia) (3–5 min at 150 W), then dried at room temperature on the polished Si wafers. The XRD patterns were recorded from 2 to 30°2 $\theta$  using a Phillips PW1710 diffractometer (Philips Analytical, Almelo, The Netherlands), with CuK $\alpha$  radiation, graphite monochromator (20 mA and 35 kV), step size 0.02°2 $\theta$ , and a counting time of 5 s per step. The resulting 001 XRD peaks of illite were used for the calculation of the mean thickness ( $T_{\text{MEAN}}$ ) and the crystallite thickness distribution (CTD) of fundamental illite

particles by Bertaut-Warren–Averbach (BWA) analysis (Drits et al., 1998) using the computer program *Mud-Master* (Eberl et al., 1996). The PVP-expandability ( $S_{\text{PVP}}$ ) was calculated from the mean thicknesses of fundamental particles according to Środoń et al. (1992).

The chemical composition was determined at Bureau Veritas Commodities, Canada Ltd. (Vancouver, British Columbia, Canada) by inductively coupled plasma optical emission spectroscopy (ICP-OES) analysis after the digestion of samples by lithium metaborate fusion followed by nitric acid leaching. The structural formulae of illite-smectites were calculated from the ICP-OES analyses (<2  $\mu\text{m}$  size fractions). Prior to calculation of structural formulae, the chemical analyses obtained for the <2  $\mu\text{m}$  size fractions were corrected for mineral impurities. The percentages of  $\text{SiO}_2$ ,  $\text{Al}_2\text{O}_3$ ,  $\text{K}_2\text{O}$ , and  $\text{Na}_2\text{O}$  corresponding to the amounts of plagioclase (albite), K-feldspar (orthoclase), and kaolinite quantified by QXRD analysis in the samples (<2  $\mu\text{m}$  size fractions) were subtracted from the chemical analyses. The procedure for calculating the structural formulae followed Čičel and Komadel (1994) and Bain and Smith (1994). The calculation for illite-smectite was based on the unit cell with 44 negative charges. Briefly, the weight percentage of each oxide was divided by its molecular weight to yield moles of oxide. Moles for each oxide were multiplied by the number of positive charges per oxide to produce the number of gram equivalents of the cation. The charge from the anion network was divided by the total of the gram equivalents of all cations to produce a proportionality factor. The gram equivalents for each cation was multiplied by the proportionality factor and divided by the valence of the cation to produce the number of cations in the unit cell. All  $\text{Si}^{4+}$  ions were assigned to tetrahedral sites and the remaining sites were filled with  $\text{Al}^{3+}$ . The remaining  $\text{Al}^{3+}$ ,  $\text{Fe}^{3+}$ , and  $\text{Mg}^{2+}$  were assigned to the octahedral sites. Excess  $\text{Mg}^{2+}$  and any  $\text{Ca}^{2+}$ ,  $\text{Na}^+$ , and  $\text{K}^+$  were assigned to the inter-layer sites.

The cation exchange capacity (CEC) was determined using the copper(II) triethylenetetramine [ $\text{Cu}(\text{Trien})$ ] $^{2+}$  method (Meier & Kahr, 1999). Solution of [ $\text{Cu}(\text{Trien})$ ] $^{2+}$  was prepared by mixing of the solution of triethylenetetramine (Sigma-Aldrich, St. Louis, Missouri, USA) and solution of copper(II) sulfate (Sigma-Aldrich, St. Louis, Missouri, USA).

Approximately 150 mg of dried sample (105°C overnight) was mixed with 50 mL of distilled water and dispersed ultrasonically for 5 min at 150 W using an ultrasonic cleaner Tesla UC 006 DM1 (Tesla, Vráble, Czechoslovakia). Afterward, 10 mL of the 0.01 M solution of [ $\text{Cu}(\text{Trien})$ ] $^{2+}$  was added and the suspension was shaken for 1 h. The suspension was then centrifuged (4500 rpm for 20 min) and the collected supernatant was passed through a syringe filter with 0.45  $\mu\text{m}$  pores. The concentration of  $\text{Cu}^{2+}$  ions in the supernatant was determined by ultra-violet visible (UV–Vis) spectrophotometry (Evolution 220, Thermo Scientific, Madison, Wisconsin, USA) at 578 nm. The CEC values were calculated following Pentrák et al. (2012).

The infrared spectra were obtained using a Nicolet 6700 Fourier-transform infrared (FTIR) spectrometer (Thermo Scientific, Madison, Wisconsin, USA). The KBr pressed-disc technique was used to measure spectra in the mid-infrared region (4000–400  $\text{cm}^{-1}$ ). Spectra were obtained by co-addition of 128 scans at a resolution of 4  $\text{cm}^{-1}$ . Spectral manipulations were performed using the Thermo Scientific *OMNIC* software package. The assignment of the bands in the infrared spectra followed Farmer (1974).

Thermogravimetric (TG) and differential thermal analysis (DTA) were performed using a NETZSCH STA 449 F3 analyzer (NETZSCH-Gerätebau, Selb, Germany) in the temperature range 20–1000°C. For all measurements, 40 mg of sample, a heating rate of 10 K/min, and a  $\text{N}_2$  flow rate of 50 mL/min were used.

Samples were examined using a scanning electron microscope (SEM), Zeiss EVO 40 (Carl Zeiss Microscopy, Jena, Germany), operated at 15 kV with a Bruker energy dispersive X-ray (EDX) detector for elemental microanalysis. The surfaces of the samples were coated with gold film.

For transmission electron microscopy (TEM) investigation, the clay fractions (0.2–2 and <0.2  $\mu\text{m}$ ) separated from the bulk samples were embedded in resin according to the method of Tessier (1984) and Elsass et al. (1998). The ultrathin sections (~70 nm thick) were cut using a Leica Ultracut UCT microtome (Leica Aktiengesellschaft, Wien, Austria) with diamond knife. The microtome slices were captured on a lacy, carbon-coated, copper grid. High-resolution TEM (HRTEM) images were taken with a JEOL JEM-ARM 200cF microscope (JEOL, Tokyo, Japan). The thickness and basal spacing of illite-smectite particles were

measured from HRTEM images in order to calculate the maximum expandability ( $S_{\text{HRTEM-MAX}}$ ) (edge layers were assumed to be smectitic) and minimum expandability ( $S_{\text{HRTEM-MIN}}$ ) (expandability within the crystals, i.e. edge layers were ignored) according to the equations reported by Środoń et al. (1990).

## Results and Discussion

### Particle-Size Distribution

The particle-size distribution results revealed differences among the samples (Table 1). The DV19/1 and DV19/2 contained significant amounts (40–55.8 wt.%) of the coarse size fraction (>2000  $\mu\text{m}$ ). On the other hand, the samples DV19/3, DV19/4, and DV19/5 were enriched in the finer size fractions (mainly 2–63  $\mu\text{m}$ ). The clay fraction (<2  $\mu\text{m}$ ) content varied between 14.5 and 49.8 wt.% for the studied samples. The largest amount of the clay fraction (<2  $\mu\text{m}$ ) was determined for the DV19/3 (49.8 wt.%). The rest of the studied samples (DV19/1, DV19/2, DV19/4, and DV19/5) contained substantially less of the <2  $\mu\text{m}$  fraction (14.5–25.1 wt.%). Interestingly, the amounts of the 0.2–2  $\mu\text{m}$  fraction were similar to those of <2  $\mu\text{m}$  fraction and in none of the samples did the <0.2  $\mu\text{m}$  content exceed 2.5 wt.% of the total weight of the samples (Table 1).

Generally, greater amounts of the clay (<2  $\mu\text{m}$ ) fractions were expected in the studied bulk K-bentonites due to relatively large illite-smectite contents in the bulk samples (37–91 wt.%, Table 2). Nevertheless, the amounts of the <2  $\mu\text{m}$  fractions for the studied K-bentonites were similar to the <2  $\mu\text{m}$  contents determined for smectite-bearing rocks from bentonite deposits in the vicinity of the K-bentonite Dolná Ves deposit

(Górniak et al., 2016, 2017; Osacký et al., 2019). The aggregation of clay particles (<2  $\mu\text{m}$ ) into larger clay aggregates explains smaller amounts of <2  $\mu\text{m}$  fractions for the studied samples. Indeed, the significant amount (45–75 wt.% of the total sample weight) of clay-bearing aggregates (2–63  $\mu\text{m}$  in size), containing 63–88 wt.% of illite-smectite, was found for the DV19/3, DV19/4, and DV19/5 samples (Tables 1, 2).

Various technological behaviors are expected for the raw materials studied during the tilemaking process due to the wide range of particle-size distributions among the samples studied (Table 1). The best tilemaking performance is expected for the DV19/3 sample which consist of ~50 wt.% of the <2  $\mu\text{m}$  clay fraction and only ~5 wt.% of sandy (>63  $\mu\text{m}$ ) fraction. All other samples contain ~15–20 wt.% of the clay fraction (<2  $\mu\text{m}$ ) and very variable amounts (~3–74 wt.%) of sandy fraction (>63  $\mu\text{m}$ ). The samples which performed most poorly, in terms of the the ceramics industry, was DV19/1, mainly due to the large amount (~74 wt.%) of coarse-grained fraction (>63  $\mu\text{m}$ ) dominated by quartz, and the small amount (~15 wt.%) of the fine-grained fraction (<2  $\mu\text{m}$ ) consisting of illite-smectite. The performance of several samples (DV19/3, DV19/4, and DV19/5) which contained substantial amounts of clay-bearing aggregates (2–63  $\mu\text{m}$ ) can be improved by more aggressive milling and maturation of raw materials. The disruption of the clay aggregates increases the plasticity which should have a positive effect on the behavior of the final bodies during tilemaking (Azzi et al., 2016).

### Mineralogical Composition

The XRD analysis showed that the samples studied consisted mainly of illite-smectite, quartz, feldspars (K-feldspar and plagioclase) and sometimes

**Table 1** The particle-size distribution (wt.%) of the K-bentonite samples

Sample	Size fraction ( $\mu\text{m}$ )						
	>2000	500–2000	63–500	2–63	<2	0.2–2	<0.2
DV19/1	55.8	3.2	14.8	11.7	14.5	14.2	0.3
DV19/2	40	2.8	6.5	25.6	25.1	23.9	1.2
DV19/3	0	2.4	2.8	45	49.8	47.3	2.5
DV19/4	0.1	0.7	1.7	78.3	19.2	16.9	2.3
DV19/5	4.7	2.2	15.5	55.5	22.1	20.6	1.5

**Table 2** Mineralogical composition (wt.%) of the bulk and various size fractions of the K-bentonite samples and special clay illite-smectite ISCz-1

Sample	Size fractions ( $\mu\text{m}$ )	Quartz	K-feldspar	Plagioclase	Illite-smectite	Kaolinite	Goethite	Anatase	Opal-CT
DV19/1	Bulk	61	1	<1	37	0	0	0	0
DV19/1	>2000	71	1	0	28	0	0	0	0
DV19/1	500–2000	75	8	0	17	0	0	0	0
DV19/1	63–500	88	3	0	9	0	0	0	0
DV19/1	2–63	83	0	<1	16	0	0	0	0
DV19/1	<2	0	0	1	99	0	0	0	0
DV19/1	0.2–2	0	0	2	98	0	0	0	0
DV19/2	Bulk	48	0	1	51	0	0	0	0
DV19/2	>2000	84	1	0	15	0	0	0	0
DV19/2	500–2000	80	1	0	19	0	0	0	0
DV19/2	63–500	79	0	<1	20	0	0	0	0
DV19/2	2–63	55	0	1	44	0	0	0	0
DV19/2	<2	0	0	1	99	0	0	0	0
DV19/2	0.2–2	0	1	3	96	0	0	0	0
DV19/3	Bulk	2	5	2	91	0	0	0	0
DV19/3	500–2000	10	81	0	9	0	0	0	0
DV19/3	63–500	21	66	0	13	0	0	0	0
DV19/3	2–63	8	2	2	88	0	0	0	0
DV19/3	<2	0	3	2	95	0	0	0	0
DV19/3	0.2–2	0	4	2	94	0	0	0	0
DV19/4	Bulk	11	0	1	88	0	0	0	0
DV19/4	500–2000	42	0	0	34	1	18	2	3
DV19/4	63–500	78	0	0	18	0	2	<1	1
DV19/4	2–63	15	0	1	84	0	0	0	0
DV19/4	<2	0	0	2	97	<1	0	0	0
DV19/4	0.2–2	0	0	1	98	1	0	0	0
DV19/5	Bulk	31	6	0	63	0	0	0	0
DV19/5	>2000	66	6	0	28	0	0	0	0
DV19/5	500–2000	74	6	0	20	0	0	0	0
DV19/5	63–500	73	5	0	22	0	0	0	0
DV19/5	2–63	33	4	0	63	0	0	0	0
DV19/5	<2	0	4	<1	95	0	0	0	0
DV19/5	0.2–2	0	4	0	96	0	0	0	0
ISCz-1	<2	2	4	0	93	<1	0	0	0

(for DV19/4 only) goethite, opal-CT, anatase, and kaolinite. Although the studied samples contained similar mineral constituents, the amount of these mineral phases varied among the samples and various size fractions. The results of quantitative XRD (QXRD) analysis for bulk and various size fractions of K-bentonites are reported in Table 2. The bulk K-bentonites (Fig. 2) contained 37–91 wt.% of illite-smectite, 2–61 wt.% of quartz and 1–7 wt.% of

feldspars. The bulk DV19/3 and DV19/4 contained substantially more illite-smectite (88–91 wt.%) than the bulk DV19/2 and DV19/5 (51–63 wt.%). The smallest illite-smectite content (37 wt.%) from the bulk samples was observed for sample DV19/1. From a technological point of view, samples DV19/3 and DV19/4 represented the type I (high-grade) K-bentonites, whereas the rest (DV19/1, DV19/2, and DV19/5) were attributed to the type II (low-grade)



K-bentonites. The coarse size fractions (>2000, 500–2000, and 63–500  $\mu\text{m}$ ) were dominated by non-clay minerals, in particular quartz (42–88 wt.% of quartz for DV19/1, DV19/2, DV19/4, and DV19/5, Table 2) or K-feldspar (66–81 wt.% of K-feldspar for DV19/3, Table 2). The amount of illite-smectite varied between 9 and 34 wt.% in the coarse fractions (>2000, 500–2000, and 63–500  $\mu\text{m}$ ) of the studied samples. The coarse fractions of DV19/4 (500–2000 and 63–500  $\mu\text{m}$ ) also contained an admixture of goethite (2–18 wt.%), opal-CT (up to 3 wt.%), anatase (up to 2 wt.%), and kaolinite (up to 1 wt.%). The clay fractions (<2  $\mu\text{m}$ ) of all samples contained  $\geq 95$  wt.% of illite-smectite. No significant changes in the mineralogy were found between the <2 and 0.2–2  $\mu\text{m}$  size fractions of the studied samples. The QXRD analysis was not performed for the finest size fractions (<0.2  $\mu\text{m}$ ) due to insufficient amounts of material.

The XRD patterns of oriented air-dried and ethylene glycolated (EG) preparations (0.2–2 and <0.2  $\mu\text{m}$ ) are shown in Fig. 3. In all XRD oriented patterns only diffraction peaks of illite-smectite were present. The differences in the position and intensity of diffraction reflections among the individual samples in the EG-solvated XRD patterns were mainly associated with the different expandability of the studied illite-smectites (the expandability results are reported in the chapter *Expandability*). The comparison of EG-solvated XRD patterns for the 0.2–2

and <0.2  $\mu\text{m}$  size fractions revealed similar positions for the illite-smectite reflections; the intensity of all reflections was less for the <0.2  $\mu\text{m}$  fractions, however, probably due to the smaller ( $a$ ,  $b$  dimensions) and in particular thinner ( $c$  dimension) crystallites of illite-smectite. The Reichweite (ordering type of illite-smectite) was determined by the position of the reflection between 5 and  $8.5^\circ 2\theta$  in EG-solvated XRD patterns (Moore & Reynolds, 1997). The reflection at  $6.7^\circ 2\theta$  ( $d=13.21$  Å) indicated the presence of R1 illite-smectite for type I K-bentonites (DV19/3 and DV19/4). The reflection between  $7.3$  and  $7.5^\circ 2\theta$  ( $d=11.79$ – $12.11$  Å) indicated the long-range ordering  $R > 1$  for illite-smectites from type II K-bentonites (DV19/1, DV19/2, and DV19/5) (Fig. 3).

The purity (mineral composition) is one of the key parameters determining the quality and, therefore, possible applications of raw materials. It should be emphasized that the whole-rock samples, DV19/3 and DV19/4 (type I K-bentonites), are of very high purity, containing between 88 and 91 wt.% of illite-smectite. Another characteristic feature of K-bentonites from the Dolná Ves deposit is that illite-smectite is practically the only clay mineral constituent of K-bentonites. The high-quality white bentonites, which are also rare in nature, find use not only in traditional applications but can be used in applications with significant added value, e.g. ceramics, detergents, pharmaceuticals, cosmetics, paint, paper, etc. (Allo & Murray, 2004). Bulk DV19/1, DV19/2, and DV19/5 samples (type II K-bentonites) contain elevated amounts (37–63 wt.%) of non-clay admixtures (mostly quartz). These may render such samples unsuitable for certain applications such as pharmaceuticals and cosmetics. On the other hand, laboratory separation of the clay fraction (<2  $\mu\text{m}$ ) by gravitational settling in a water column decreased the amount of non-clay admixtures for all <2  $\mu\text{m}$  size samples to  $\leq 5$  wt.% (Table 2).

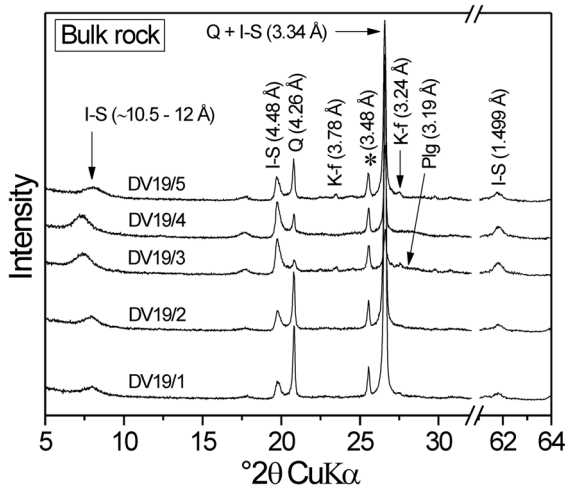


**Fig. 2** XRD patterns of random preparations for bulk K-bentonites. I-S – illite-smectite, Q – quartz, K-f – K-feldspar, Plg – plagioclase, and \* – corundum (internal standard)

### Chemical Composition

The chemical composition of the K-bentonites studied (bulk and <2  $\mu\text{m}$ ) is reported in Table 3. The large amounts of  $\text{SiO}_2$  and  $\text{Al}_2\text{O}_3$  were associated with the main mineral constituents of the samples, quartz and illite-smectite, respectively. The significant positive correlations ( $p < 0.0001$ ,  $R^2 = 0.990$  and  $0.975$ ) established between the chemical composition (ICP-OES analysis) and mineral composition (QXRD analysis)

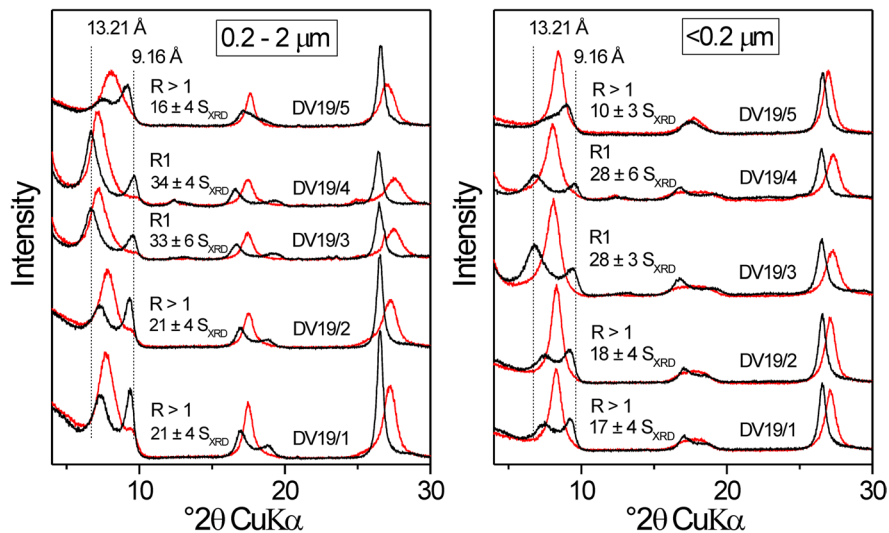


**Fig. 3** XRD patterns of oriented air-dried (red) and ethylene glycolated (black) preparations for the 0.2–2  $\mu\text{m}$  (left) and <0.2  $\mu\text{m}$  (right) fractions of K-bentonites.  $S_{\text{XRD}}$  – percentage of smectite interlayers (expandability), R1 and R > 1 – ordering type (Reichweite) of illite-smectite

confirmed that the variability in the  $\text{SiO}_2$  and  $\text{Al}_2\text{O}_3$  contents among the samples was due to the various amounts of quartz and illite-smectite (Fig. 4). The results showed that the  $\text{SiO}_2$  and  $\text{Al}_2\text{O}_3$  contents increased gradually with increasing amounts of quartz and illite-smectite, respectively. For bulk K-bentonites, significant positive correlations were also observed for the LOI (loss-on-ignition) with the amount of illite-smectite, and  $\text{K}_2\text{O}$  content with the amount of illite-smectite + K-feldspar (Fig. 4). With the larger LOI and  $\text{K}_2\text{O}$ , the amount of illite-smectite increased in the bulk samples, a small contribution of K-feldspar to the  $\text{K}_2\text{O}$  content was found in particular for samples DV19/3 and DV19/5. The mineralogical compositions of the K-bentonites had a significant effect on the LOI and  $\text{K}_2\text{O}$  for the bulk samples whereas the impact of mineralogical compositions on the LOI and  $\text{K}_2\text{O}$  was suppressed for the <2  $\mu\text{m}$  size fraction samples, due mainly to a similar amount of illite-smectite (95–99 wt.% of illite-smectite, Table 2). The values for  $\text{K}_2\text{O}$  and LOI for the <2  $\mu\text{m}$  size fractions of K-bentonites were controlled not only by the mineralogical composition, but, in particular, by the expandability of illite-smectite. With increasing expandability of the illite-smectites, the  $\text{K}_2\text{O}$  content decreased and LOI increased (Tables 3, 4). The main source of  $\text{Fe}_2\text{O}_3$ , MgO, CaO, and  $\text{Na}_2\text{O}$  was probably illite-smectite; a small contribution of

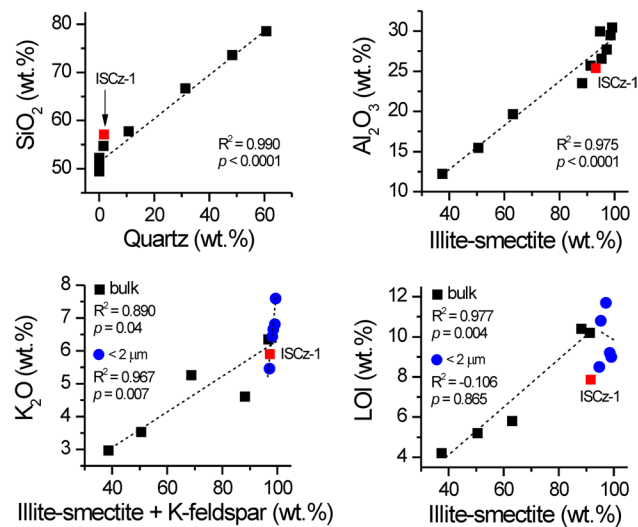
plagioclase was also possible mainly due to the  $\text{Na}_2\text{O}$  and CaO contents, however.

The use of clays in tile manufacturing depends on the technological and appearance requirements of the ceramic body. The color of the ceramic body after firing is probably one of the most important parameters. This color depends essentially on the chemical composition which is intimately connected with the mineralogy of the clayey raw materials. Based on the color after firing, the ceramic bodies are distinguished as light-firing (from white to light brown) and dark-firing (from pink to dark brown) clays according to an  $\text{Fe}_2\text{O}_3$  threshold of 3 wt.% (Dondi et al., 2014). All of the K-bentonite samples studied displayed  $\text{Fe}_2\text{O}_3$  contents of <3 wt.%; thus, they can be considered as light-firing clays. The smallest amount of  $\text{Fe}_2\text{O}_3$  (0.98–0.99 wt.%) was observed for sample DV19/3 (type I K-bentonite). Some researchers pointed out that not only is the absolute  $\text{Fe}_2\text{O}_3$  content important but also the mineralogical phase in which the Fe is bound (e.g. Fe oxyhydroxides versus clay minerals) (Christidis & Scott, 1997). For most of the studied samples the Fe was primarily present in the octahedral sheets of illite-smectite. The only exception was the DV19/4 sample for which a variable amount of goethite admixture was detected by XRD, mainly in the coarse size fractions. The DV19/4 K-bentonite can be recognized visually at the deposit because of

**Table 3** Chemical compositions (wt.%), illite-smectite structural formulae, and illite-smectite octahedral ( $\xi_{\text{Oct}}$ ), tetrahedral ( $\xi_{\text{Tet}}$ ), and total ( $\xi_{\text{Tot}}$ ) layer charges

Sample	SiO <sub>2</sub>	Al <sub>2</sub> O <sub>3</sub>	Fe <sub>2</sub> O <sub>3</sub>	MgO	CaO	Na <sub>2</sub> O	K <sub>2</sub> O	TiO <sub>2</sub>	P <sub>2</sub> O <sub>5</sub>	MnO	LOI	Total
Bulk												
DV19/1	78.56	12.24	1.28	0.35	0.12	0.02	2.97	0.08	<0.01	0.02	4.2	99.84
DV19/2	73.60	15.46	1.45	0.29	0.12	0.03	3.53	0.10	<0.01	0.02	5.2	99.80
DV19/3	54.74	25.7	0.99	2.13	0.15	0.01	6.35	0.16	0.02	<0.01	10.2	99.82
DV19/4	57.81	23.52	1.32	1.9	0.11	0.02	4.61	0.15	0.01	<0.01	10.4	99.85
DV19/5	66.66	19.66	1.68	0.41	0.14	0.03	5.26	0.12	0.01	0.04	5.8	99.81
Clay fraction (<2 μm)												
DV19/1	50.26	29.50	2.75	0.91	0.24	0.10	6.66	0.11	0.06	0.05	9.2	99.84
DV19/2	49.50	30.47	2.72	0.64	0.23	0.15	6.81	0.11	0.05	0.04	9	99.72
DV19/3	52.25	26.57	0.98	2.33	0.19	0.06	6.44	0.14	0.03	<0.01	10.8	99.79
DV19/4	50.22	27.70	1.73	2.23	0.17	0.16	5.46	0.26	0.08	0.01	11.7	99.72
DV19/5	49.67	29.97	2.4	0.70	0.24	0.28	7.59	0.11	0.24	0.06	8.5	99.76
*ISCz-1	57.06	25.39	1.67	2.25	0.03	0.74	5.93	0.11	0.02	n.d	7.9	101.12
Structural formulae and layer charges ( $\xi$ )												
DV19/1	$\text{K}_{1.18}\text{Mg}_{0.04}\text{Ca}_{0.03}(\text{Al}_{3.57}\text{Fe}_{0.28}\text{Mg}_{0.14})(\text{Si}_{6.82}\text{Al}_{1.18})\text{O}_{20}(\text{OH})_4$									$\xi_{\text{Oct}}$	$\xi_{\text{Tet}}$	$\xi_{\text{Tot}}$
DV19/2	$\text{K}_{1.18}\text{Mg}_{0.06}\text{Ca}_{0.03}\text{Na}_{0.01}(\text{Al}_{3.64}\text{Fe}_{0.28}\text{Mg}_{0.08})(\text{Si}_{6.71}\text{Al}_{1.29})\text{O}_{20}(\text{OH})_4$									0.14	1.18	1.32
DV19/3	$\text{K}_{0.99}\text{Mg}_{0.10}\text{Ca}_{0.03}(\text{Al}_{3.50}\text{Mg}_{0.39}\text{Fe}_{0.11})(\text{Si}_{7.14}\text{Al}_{0.86})\text{O}_{20}(\text{OH})_4$									0.08	1.29	1.37
DV19/4	$\text{K}_{0.98}\text{Mg}_{0.16}\text{Ca}_{0.03}(\text{Al}_{3.51}\text{Mg}_{0.31}\text{Fe}_{0.18})(\text{Si}_{6.95}\text{Al}_{1.05})\text{O}_{20}(\text{OH})_4$									0.39	0.86	1.25
DV19/5	$\text{K}_{1.27}\text{Na}_{0.05}\text{Ca}_{0.04}\text{Mg}_{0.02}(\text{Al}_{3.61}\text{Fe}_{0.26}\text{Mg}_{0.13})(\text{Si}_{6.69}\text{Al}_{1.31})\text{O}_{20}(\text{OH})_4$									0.31	1.05	1.36
*ISCz-1	$\text{K}_{0.95}\text{Na}_{0.20}(\text{Al}_{3.35}\text{Mg}_{0.47}\text{Fe}_{0.18})(\text{Si}_{7.32}\text{Al}_{0.68})\text{O}_{20}(\text{OH})_4$									0.13	1.31	1.44
										0.47	0.68	1.15

\* from Geramian et al. (2016)

**Fig. 4** SiO<sub>2</sub>, Al<sub>2</sub>O<sub>3</sub>, and K<sub>2</sub>O contents and LOI (loss-on-ignition) plotted versus the amount of quartz, illite-smectite, and sum of illite-smectite and K-feldspar

**Table 4** The expandabilities (%) for various clay fractions of the samples studied

Sample	$S_{XRD}$		$S_{PVP}$		$S_{SF}$	$S_{HRTEM-MAX}$		$S_{HRTEM-MIN}$		$n$
	<2 $\mu m$	0.2–2 $\mu m$	<0.2 $\mu m$	>2 $\mu m$		<2 $\mu m$	0.2–2 $\mu m$	<0.2 $\mu m$	>2 $\mu m$	
DV19/1	22 ± 4	21 ± 4	17 ± 4	34	34	31	32	32	31	32
DV19/2	22 ± 4	21 ± 4	18 ± 4	33	34	31	32	32	31	32
DV19/3	35 ± 5	33 ± 6	28 ± 3	37	38	42	43	43	42	43
DV19/4	35 ± 5	34 ± 4	28 ± 6	42	42	36	43	43	36	43
DV19/5	16 ± 3	16 ± 4	10 ± 3	29	28	25	28	28	25	28
ISCz-1	25 ± 5						45			

$S_{XRD}$  expandability determined from ethylene glycolated XRD patterns,  $S_{PVP}$  expandability calculated from samples intercalated with polyvinylpyrrolidone,  $S_{SF}$  expandability determined from K content per half unit cell in illite-smectite,  $S_{HRTEM-MAX}$  maximum expandability calculated from HRTEM data,  $S_{HRTEM-MIN}$  minimum expandability calculated from HRTEM data;  $n$ —number of measured particles

its pale orange color (probably due to goethite admixture). In addition, the bulk and <2  $\mu m$  size fraction of DV19/4 K-bentonite displayed substantially higher concentrations of some minor elements such as As (105.5–106.7 ppm), Pb (52.3–56.6 ppm), and Hg (0.35–0.86 ppm) in comparison with the rest of the studied samples (Table S2). The elevated amounts of these elements can make the DV19/4 K-bentonite unsuitable for potential applications in pharmacy, cosmetics, and the food industry (Allo & Murray, 2004).

The position of the 060 reflection of illite-smectite near 1.499 Å indicated the presence of dioctahedral illite-smectite in all the studied samples (Fig. 2). The structural formulae of illite-smectites were calculated from the chemical analyses (<2  $\mu m$  size fractions) corrected for mineral impurities (Table 3). The formulae showed that the layer charge ( $\xi$ ) of all studied illite-smectites arose mainly from the Al-for-Si substitutions in the tetrahedral sheet ( $\xi_{tet} = 0.86–1.31$ , Table 3). The substantially smaller octahedral layer charge ( $\xi_{oct} = 0.08–0.39$ , Table 3) was related mainly to the substitution of Mg for Al. Due to the elevated octahedral Mg content, the illite-smectites with the greatest XRD expandability ( $S_{XRD} = \sim 28–35\%$  for DV19/3 and DV19/4, Table 4), arising from the type I K-bentonites, had substantially greater octahedral charge ( $\xi_{oct} = 0.31–0.39$ , Table 3) compared to the illite-smectites with the lesser XRD expandability ( $S_{XRD} = \sim 10–22\%$ ,  $\xi_{oct} = 0.08–0.14$  for DV19/1, DV19/2 and DV19/5, Tables 3 and 4), coming from the type II K-bentonites. The illite-smectites from the type I K-bentonites (DV19/3 and DV19/4) had greater octahedral Mg (0.31–0.39 Mg per  $O_{20}(OH)_4$ ) and smaller octahedral Fe contents (0.11–0.18 Fe per  $O_{20}(OH)_4$ ) in comparison with the illite-smectites from the type II K-bentonites (DV19/1, DV19/2 and DV19/5) in which the opposite trend was observed; greater octahedral Fe (0.26–0.28 Fe per  $O_{20}(OH)_4$ ) and lesser octahedral Mg (0.08–0.14 Mg per  $O_{20}(OH)_4$ ) contents (Table 3). The amount of K cations in the interlayer space of all illite-smectites increased with the lower  $S_{XRD}$  value (Fig. 5). The swelling (smectitic) interlayers in illite-smectites were occupied by Ca, Mg, and sometimes Na (Table 3). The crystal chemistry of the reference Special clay ISCz-1 illite-smectite was similar to the DV19/3 (type I K-bentonite).

## Fourier-Transform Infrared Spectroscopy (FTIR)

The FTIR spectra of two clay fractions (0.2–2 and <0.2  $\mu\text{m}$ ) for the studied K-bentonites are shown in Fig. 6. Note that the clay fractions of K-bentonites contained  $\geq 94$  wt.% of illite-smectite; therefore, almost all absorption bands observed in the FTIR spectra were associated with the illite-smectite. No significant spectral changes were observed among the samples in the OH-stretching region (3800–3200  $\text{cm}^{-1}$ ). The absorption bands near 3625  $\text{cm}^{-1}$  and 3420  $\text{cm}^{-1}$  present in the spectra of all samples were attributed to the OH-stretching vibrations of structural hydroxyl groups and water molecules, respectively (Fig. 6). The only difference among the studied samples in this infrared region was the presence of a small band at 3699  $\text{cm}^{-1}$  for both of the clay fractions (0.2–2 and <0.2  $\mu\text{m}$ ) of sample DV19/4, which indicated the admixture of kaolinite (Fig. 6g, h). A small amount of kaolinite ( $\sim 1$  wt.%) was also confirmed in the clay fractions of DV19/4 by XRD analysis (Table 2).

The more pronounced spectral changes were found among the samples in the 950–700  $\text{cm}^{-1}$  region. The strong bands near 820  $\text{cm}^{-1}$  and 756  $\text{cm}^{-1}$  in the spectra of illite-smectites (0.2–2 and <0.2  $\mu\text{m}$ ) from the type II K-bentonites (DV19/1, DV19/2, and DV19/5) (Fig. 6a–d, i, j) attributed to the tetrahedral Al–O out-of-plane and Al–O–Si in-plane vibrations, respectively, were related to the illitic component within the mixed-layer structure of illite-smectite (Madejová & Komadel, 2001). In the spectra of illite-smectites (0.2–2 and <0.2  $\mu\text{m}$ ) from the type I K-bentonites (DV19/3 and DV19/4), the intensity of these bands (820  $\text{cm}^{-1}$  and 756  $\text{cm}^{-1}$ ) was less than that from the type II K-bentonite samples. In addition, the band near 845  $\text{cm}^{-1}$ , assigned to the vibrations of AlMgOH

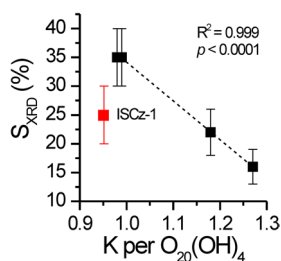


**Fig. 5** XRD expandability ( $S_{\text{XRD}}$ ) plotted versus K content per unit cell in the illite-smectites and reference illite-smectite ISCz-1

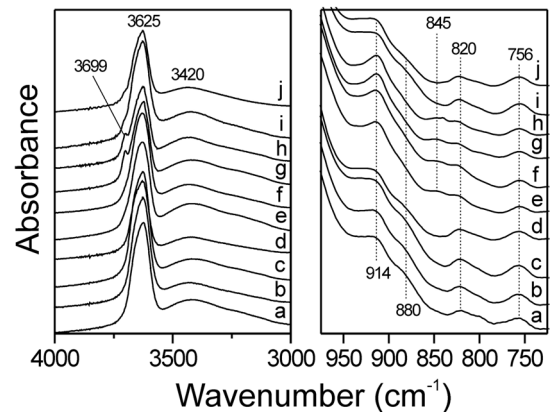


**Fig. 6** FTIR spectra of the 0.2–2  $\mu\text{m}$  fractions for **a** DV19/1, **c** DV19/2, **e** DV19/3, **g** DV19/4, **i** DV19/5; and <0.2  $\mu\text{m}$  fractions for **b** DV19/1, **d** DV19/2, **f** DV19/3, **h** DV19/4, **j** DV19/5

groups, occurred in the spectra of illite-smectites (0.2–2 and <0.2  $\mu\text{m}$ ) from the type I K-bentonites (DV19/3 and DV19/4) (Fig. 6e–h). The presence of the AlMgOH band corresponded well with the greater octahedral Mg content for illite-smectites of the technological type I (DV19/3 and DV19/4) determined from the chemical analyses (Table 3). Similarly, the small inflection near 880  $\text{cm}^{-1}$  (AlFeOH) observed in the spectra of DV19/1, DV19/2, and DV19/5 illite-smectites (0.2–2 and <0.2  $\mu\text{m}$ ) indicated elevated amounts of octahedral Fe for illite-smectites of the type II, which was also in line with the illite-smectite structural formulae calculated from the chemical analyses (Table 3). Other spectral changes were observed for distinct technological types of illite-smectites in the form of AlAlOH bending vibrations. In the spectra of type I illite-smectites (0.2–2 and <0.2  $\mu\text{m}$ ) (DV19/3 and DV19/4), the AlAlOH vibration band was intense and well resolved at 914  $\text{cm}^{-1}$ , whereas in the spectra of type II illite-smectites (0.2–2 and <0.2  $\mu\text{m}$ ) (DV19/1, DV19/2, and DV19/5), the AlAlOH band appeared as a broad shoulder of lower intensity (Fig. 6a–d, i, j).

## Scanning Electron Microcopy-Energy Dispersive X-Ray Spectroscopy (SEM–EDX)

The SEM images and corresponding EDX spectra for the main mineral constituents (illite-smectite, quartz, and K-feldspar) of K-bentonites are shown in Fig. 7.



Quartz was present in the form of larger aggregates (usually from several 10 s to several 100 s of  $\mu\text{m}$  across) consisting of well-developed crystals. K-feldspar formed large aggregates (several 100 s of  $\mu\text{m}$  in size) composed of intergrown monoclinic crystals. Illite-smectite formed thin irregular platy crystals usually between 1 and 2  $\mu\text{m}$  in diameter with an abundance of edge-to-face and face-to-face contacts. Illite-smectite often coated the surface of non-clay minerals (quartz, K-feldspar) and filled the voids and cavities within the large aggregates consisting mainly of quartz and sometimes K-feldspar crystals (Fig. 7a). This explains larger amounts of illite-smectite (9–34 wt.%) in the coarser fractions (>2000 and 500–2000  $\mu\text{m}$ ) of K-bentonites (Table 2).

#### Bertaut-Warren–Averbach (BWA) Analysis and High-Resolution Transmission Electron Microscopy (HRTEM) Measurements

The BWA results showed a lognormal shape of the crystallite thickness distributions (CTDs) for all the studied samples (Fig. 8). The maxima of the CTDs decreased gradually in frequency, broadened, and shifted to greater thickness with increasing mean thickness ( $T_{\text{MEAN}}$ ) of the samples. No significant changes in the calculated  $T_{\text{MEAN}}$  values were found between the <2  $\mu\text{m}$  and 0.2–2  $\mu\text{m}$  size fractions (Table 5). The <0.2  $\mu\text{m}$  size fractions of all samples displayed slightly greater  $T_{\text{MEAN}}$  values compared to the 0.2–2  $\mu\text{m}$  size fractions (except DV19/3) (Table 5). A clear inverse relationship was found between the  $T_{\text{MEAN}}$  values and the XRD expandabilities ( $S_{\text{XRD}}$ ). The illite-smectite from the type II K-bentonite (DV19/5) with the lowest expandability ( $S_{\text{XRD}} = \sim 10\text{--}16\%$ ) had a  $T_{\text{MEAN}}$  of 3.5–4 nm, whereas the illite-smectites from the type I K-bentonite (DV19/3 and DV19/4) with the greatest expandabilities ( $S_{\text{XRD}} = \sim 28\text{--}35\%$ ) had a  $T_{\text{MEAN}}$  of 2.4–2.8 nm (Tables 4 and 5). A similar relationship between the  $S_{\text{XRD}}$  and the  $T_{\text{MEAN}}$  values determined by the Pt-shadowing technique for illite-smectites from the Dolná Ves deposit was reported by Šucha et al. (1996).

The HRTEM measurements of two clay fractions (0.2–2  $\mu\text{m}$  and <0.2  $\mu\text{m}$ ) of highly smectitic technological type I illite-smectite (DV19/4) and highly illitic technological type II illite-smectite (DV19/5) provided information about the number of 2:1 layers in the illite-smectite crystals (Fig. 9).

Significant differences were found for illite-smectites coming from the two technological types of K-bentonites. The distributions of the number of layers per illite-smectite particles (Fig. 9) showed that the illite-smectite of the type I (DV19/4), with greater expandability, contained substantially more of the thinner particles (mainly mono-, bi-, and tri-layers, Fig. 9a, b) compared to the illite-smectite of the type II (DV19/5), with the smallest expandability, which contained thicker particles (mainly five and six layers and thicker, Fig. 9c, d). As a consequence, the average number of layers for highly illitic type II illite-smectite (DV19/5) was 5–6, but only 3 for highly smectitic type I illite-smectite (DV19/4). No significant changes were observed in the shape of the distributions of the number of layers per illite-smectite particle and the average number of layers per illite-smectite particle for various size fractions (0.2–2  $\mu\text{m}$  and <0.2  $\mu\text{m}$ ) of DV19/4. Sample DV19/5, for which the fewest illite-smectite particles were available for measurement, showed larger discrepancies in the shape of the distributions of the number of layers and the average number of layers per particle between the 0.2–2  $\mu\text{m}$  and <0.2  $\mu\text{m}$  size fractions. These discrepancies may be due to poor statistical data, particularly in the case of the 0.2–2  $\mu\text{m}$  fraction of DV19/5 ( $n = 70$ , Table 4).

#### Expandability

The expandability ( $S$ ) (i.e. percentage of smectite interlayers) determined by several different techniques, namely, powder XRD ( $S_{\text{XRD}}$ ), transmission electron microscopy ( $S_{\text{HRTEM-MAX}}$  and  $S_{\text{HRTEM-MIN}}$ ), chemical analysis (from K contents per half unit cell in illite-smectites) ( $S_{\text{SF}}$ ), and after intercalation of samples with polymer polyvinylpyrrolidone ( $S_{\text{PVP}}$ ), are given in Table 4. Based on the expandabilities determined, the samples can be divided into three groups, samples DV19/3 and DV19/4 with the greatest expandability, DV19/1 and DV19/2 with a moderate expandability, and DV19/5 with the smallest expandability. Overall, the illite-smectites coming from the type I K-bentonites (DV19/3 and DV19/4) displayed greater expandabilities than the illite-smectites coming from the type II K-bentonites (DV19/1, DV19/2, and DV19/5).

The  $S_{\text{XRD}}$  values determined from the EG-solvated XRD patterns (<2  $\mu\text{m}$  fractions) were  $35 \pm 5\%$  for

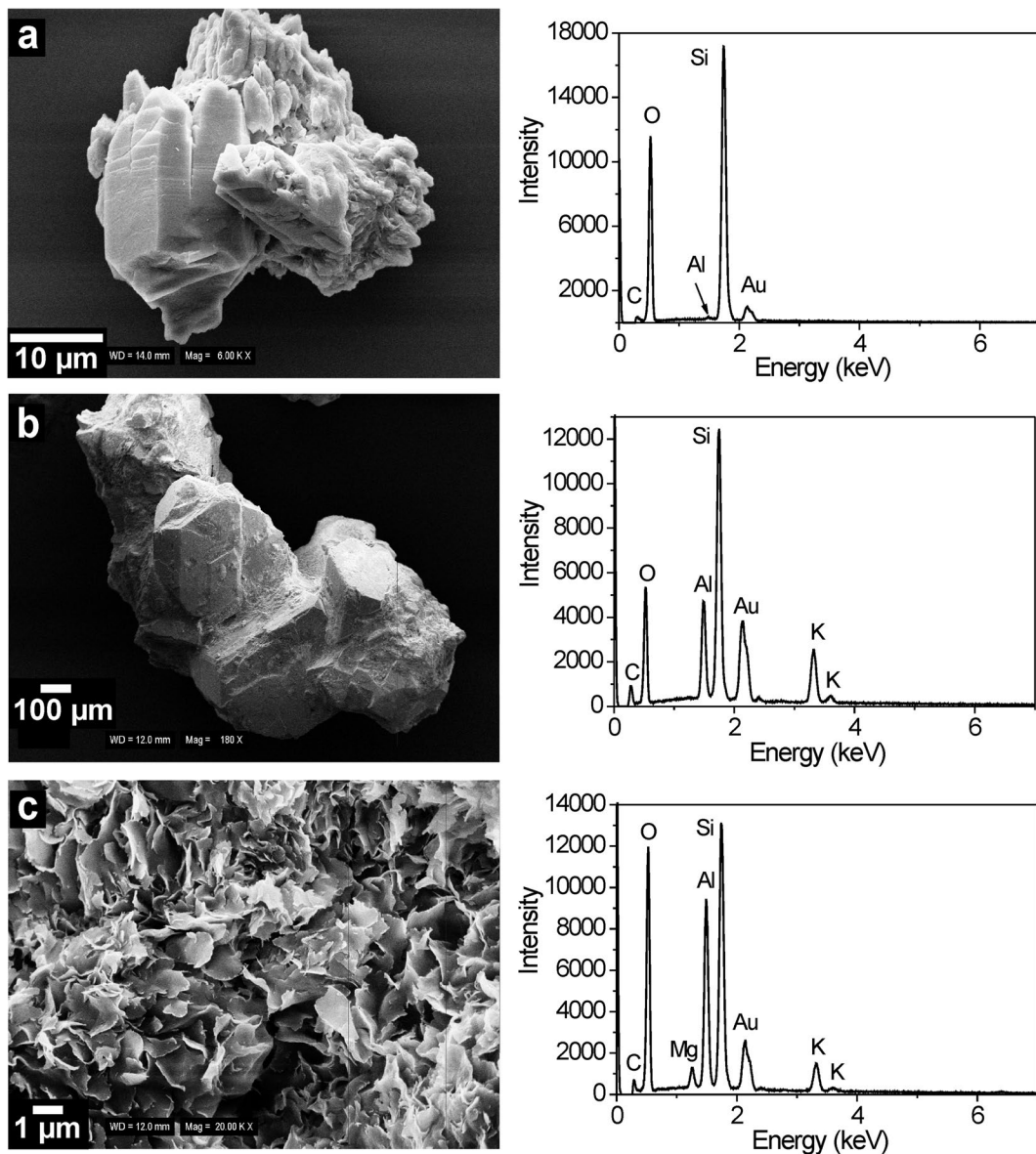


**Fig. 7** SEM images (left) and corresponding EDX spectra (right) of **a** quartz, **b** K-feldspar, and **c** illite-smectite from K-bentonite

the DV19/3 and DV19/4 and only  $16 \pm 3\%$  for the DV19/5. The  $S_{XRD}$  values for the  $<2 \mu\text{m}$  fractions of DV19/1 and DV19/2 were  $22 \pm 4\%$ , which were values similar to that determined for ISCz-1 ( $25 \pm 5\%$ ). The  $S_{XRD}$  values for the  $<2 \mu\text{m}$  and  $0.2\text{--}2 \mu\text{m}$  fractions of all samples were very similar. For the  $<0.2 \mu\text{m}$  fractions, the  $S_{XRD}$  values of all samples had a tendency to be slightly smaller but this small change was within the standard deviation error. Šucha et al. (1992) reported that illite-smectites ( $<1 \mu\text{m}$  size

fractions) from the Dolná Ves deposit had similar  $S_{XRD}$  values, ranging from 6 to 45%.

Very good agreement was found between the  $S_{PVP}$  (determined from the samples intercalated by polyvinylpyrrolidone) and  $S_{SF}$  (determined from K contents per half unit cell in illite-smectites) values (Fig. 10). In addition, both the  $S_{PVP}$  and  $S_{SF}$  values exhibited a trend similar to that observed for  $S_{XRD}$  values (Fig. 10). The only main difference was systematically greater  $S_{PVP}$  and  $S_{SF}$  values in comparison

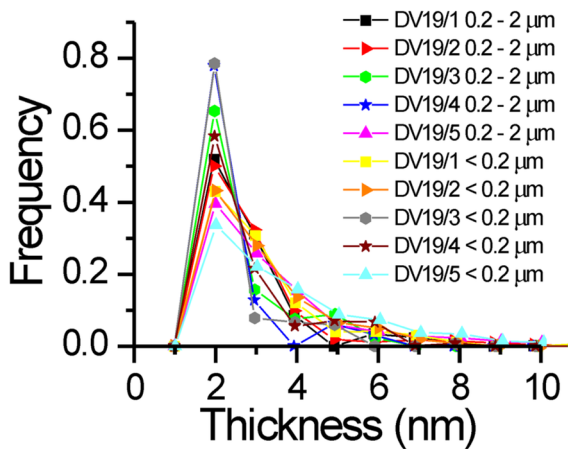


**Fig. 8** Crystallite thickness distributions of fundamental particles for the 0.2–2 and <0.2 μm fractions of the samples studied

with the  $S_{XRD}$  values. This systematic discrepancy was related to the underestimation of the expandability determined by XRD ( $S_{XRD}$ ) because the smectitic edges of illite-smectite crystals are not detected by XRD analysis (Eberl & Środoń, 1988).

From HRTEM measurements, the maximum ( $S_{HRTEM-MAX}$ ) and minimum ( $S_{HRTEM-MIN}$ ) expandabilities were calculated according to the method described by Środoń et al. (1990).  $S_{HRTEM-MIN}$  refers to the percentage of smectite interlayers located within the illite-smectite crystals. As such,  $S_{HRTEM-MIN}$  values should correspond to the  $S_{XRD}$  values because the crystal edges are ignored in the  $S_{HRTEM-MIN}$  calculation. In case of  $S_{HRTEM-MAX}$ , the illite-smectite crystal edges are assumed to be smectitic and these smectitic crystal edges are involved in the expandability calculation. Therefore,  $S_{HRTEM-MAX}$  values should correspond

to the  $S_{SF}$  and  $S_{PVP}$  (Środoń et al., 1990; Šucha et al., 1996). For the HRTEM investigation, different clay fractions (0.2–2 μm and <0.2 μm) of highly smectitic type I illite-smectite (DV19/4) and highly illitic type II illite-smectite (DV19/5) were used. Despite the limited number of samples analyzed by HRTEM, the data showed good agreement between the  $S_{XRD}$  and  $S_{HRTEM-MIN}$  values, which was also in line with the results of Środoń et al. (1990) for illite-smectites from the Upper Silesian coal basin (Poland).

Cation Exchange Capacity (CEC)

The CEC results for the bulk and various clay fractions (<2, 0.2–2, and <0.2 μm) of K-bentonites are shown in Table 5. A significant impact of illite-smectite expandability ( $S_{XRD}$ ) and illite-smectite content on the CEC values was demonstrated by significant positive correlations ( $p < 0.05$ ) established among these parameters (Fig. 11). The CEC values increased with increasing expandability and the amount of illite-smectite. Due to the high purity ( $\geq 94$  wt.% of illite-smectite) of K-bentonite clay fractions (<2 and 0.2–2 μm), the impact of the illite-smectite content was ignored and the expandability of illite-smectite was probably the primary parameter affecting the CEC values in the clay-sized fractions. As a consequence, the clay fractions (<2 μm) isolated from the type I K-bentonites had substantially greater CEC (~44–46 meq/100 g) than the corresponding fractions from the type II K-bentonites (~26–30 meq/100 g) (Table 5). The increase in  $S_{XRD}$  by ~10% corresponded to the increase in CEC by ~10 meq/100 g (Fig. 11). The CEC value of 113 meq/100 g predicted from the correlation for the fully expandable sample (pure smectite) was in excellent agreement with the CEC values determined for

**Table 5** CEC and mean crystallite thickness ( $T_{MEAN}$ ) of fundamental particles for the samples studied (bulk, <2, 0.2–2, and <0.2 μm fractions)

Sample	CEC (meq/100 g)				$T_{MEAN}$ (nm)		
	Bulk	<2 μm	0.2–2 μm	<0.2 μm	<2 μm	0.2–2 μm	<0.2 μm
DV19/1	11.8 ± 1.31	30.0 ± 0.23	28.7 ± 0.23	28.8 ± 0.22	2.9	2.9	3.2
DV19/2	12.2 ± 2.35	29.8 ± 1.11	29.5 ± 0.05	28.0 ± 0.59	3.0	2.9	3.2
DV19/3	38.0 ± 2.10	43.6 ± 0.47	41.0 ± 0.53	42.4 ± 0.12	2.7	2.6	2.4
DV19/4	40.2 ± 0.99	45.9 ± 1.01	42.8 ± 0.42	43.2 ± 1.93	2.4	2.4	2.8
DV19/5	15.8 ± 0.62	25.7 ± 1.93	23.1 ± 0.47	23.6 ± 0.27	3.5	3.6	4
ISCz-1		36.9 ± 0.13					

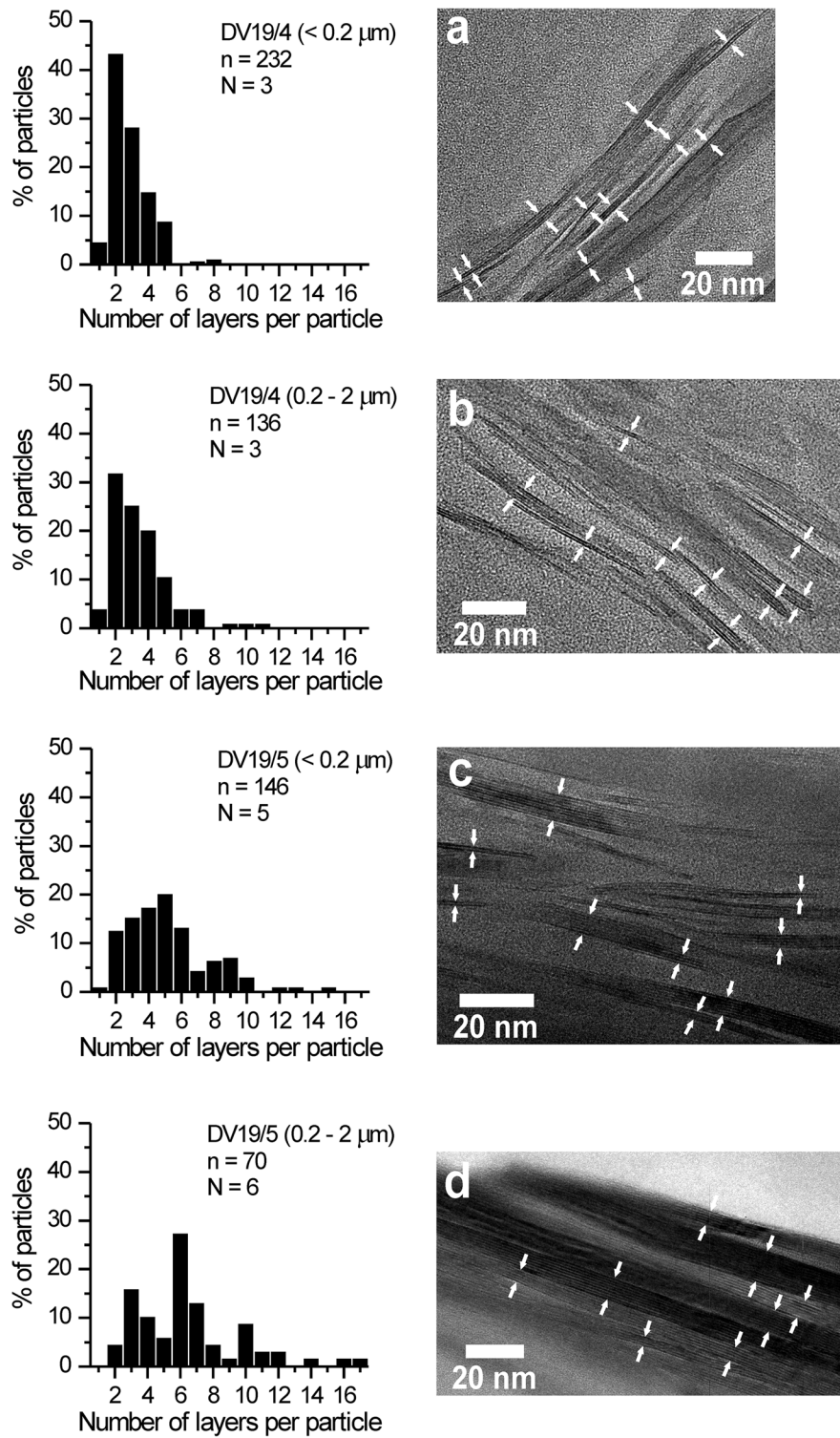


**Fig. 9** HRTEM images (right) of <0.2  $\mu\text{m}$  fractions for **a** DV19/4, **c** DV19/5; and 0.2–2  $\mu\text{m}$  fractions for **b** DV19/4, **d** DV19/5. Arrows indicate the measured cross sections of illite-smectite crystals. Corresponding distributions of numbers of layers in illite-smectite crystals (left). N—mean number of layers in sample, n—number of measured particles

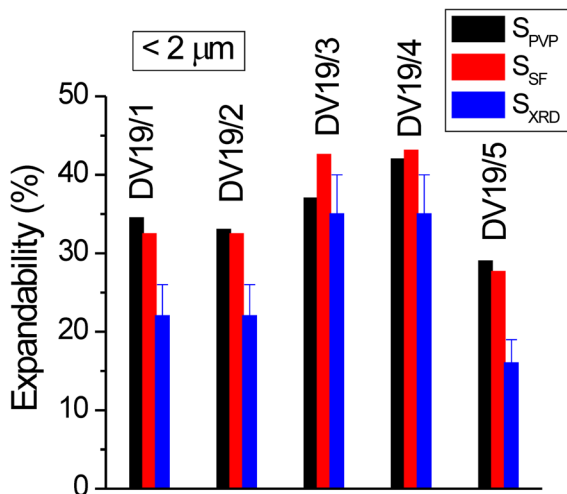


**Fig. 10** Relationships among the illite-smectite (<2  $\mu\text{m}$  size fractions) expandabilities determined by powder XRD ( $S_{XRD}$ ), chemical analysis (from K contents per half unit cell in illite-smectites) ( $S_{SF}$ ), and after intercalation of samples with polyvinylpyrrolidone ( $S_{PVP}$ )

the smectite-rich rocks from several bentonite deposits (e.g. Stará Kremnička III and Lutilla I) located in the southern part of the K-bentonite deposit at Dolná Ves (Osacký et al., 2019). The CEC determined for the <2  $\mu\text{m}$  fraction of Special clay ISCz-1 was close to 37 meq/100 g (Table 5).

#### Thermal Analysis

The thermogravimetric (TG), derivative thermogravimetric (DTG), and differential thermal analysis (DTA) curves for the 0.2–2  $\mu\text{m}$  fractions of

K-bentonites are shown in Fig. 12. These clay fractions were almost pure ( $\geq 94$  wt.%) illite-smectite samples and thus the thermal behavior observed using TG, DTG, and DTA was related mainly to the presence of illite-smectite in the samples. At low temperature (<250°C), the DTA curves of all samples showed the presence of a large endothermic event with the maximum at 86–95°C, associated with the loss of surface  $\text{H}_2\text{O}$  (e.g.  $\text{H}_2\text{O}$  on the external surfaces) and  $\text{H}_2\text{O}$  from the interlayer space of illite-smectite. The mass loss at <250°C determined on the TG curves accounted for 3.8–7.2% (Fig. 12). Due to the greater expandability of illite-smectite, the type I K-bentonite samples (DV19/3 and DV19/4) displayed much greater mass loss at <250°C (6.9–7.2%) than the type II K-bentonite samples (mass loss of 3.8–5.4% for DV19/1, DV19/2, and DV19/5). In other words, smectitic interlayers within the illite-smectite structure (i.e. greater expandability) adsorbed more  $\text{H}_2\text{O}$  causing greater mass loss at <250°C.

At higher temperatures (250–800°C), the mass loss (4.5–5.6%, Fig. 12) was related mainly to the dehydroxylation of illite-smectite. On the DTA curves, the illite-smectite dehydroxylation was indicated by broad endothermic shoulders near 500–520°C and well resolved endothermic peaks with the maximum at 660–682°C (Fig. 12). The endothermic/exothermic events on the DTA curves at ~900–950°C were due to decomposition/recrystallization of illite-smectites (Fig. 12). Illite-smectites are often characterized by the two endothermic reactions near 500°C and 700°C corresponding to

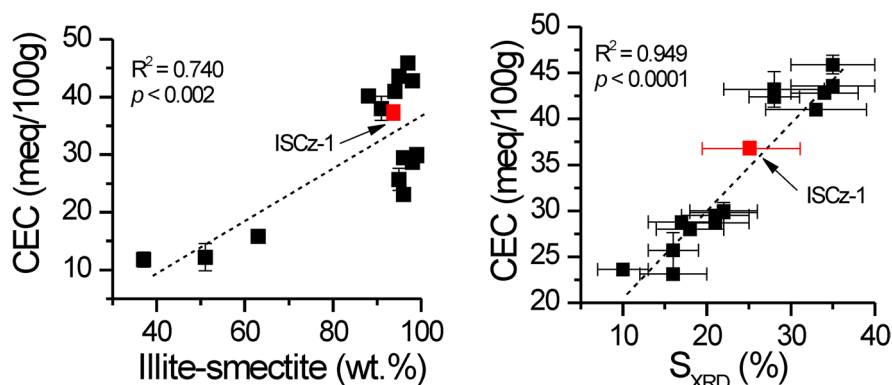


**Fig. 11** CEC plotted versus illite-smectite content (left) and XRD expandability ( $S_{XRD}$ ) (right) for K-bentonite samples and reference illite-smectite ISCz-1



the dehydroxylation of trans-vacant (*tv*) and cis-vacant (*cv*) 2:1 layers, respectively (e.g. Drits et al., 1995, 1996; Muller et al., 2000). The intensity of these peaks in the DTG curves reflect the proportions of the *tv* and *cv* 2:1 layers in a given clay mineral (Drits et al., 1995; Muller et al., 2000). Over the 250–800°C region, the DTG curves of the illite-smectites coming from the type I K-bentonites (DV19/3 and DV19/4) showed the presence of both peaks, at ~660°C and ~500°C, whereas the

illite-smectites coming from the type II K-bentonites (DV19/1 and DV19/2) displayed a more intense peak near 680°C and only a negligible inflection near 500°C (Fig. 12). This observation indicated that all illite-smectites studied consisted of both *cv* and *tv* 2:1 layers. However, the proportion of *cv* layers was greater for illite-smectites from the type II K-bentonite (DV19/1 and DV19/2), whereas for illite-smectites from the type I K-bentonite (DV19/3 and DV19/4) the proportion of *cv* layers was lower

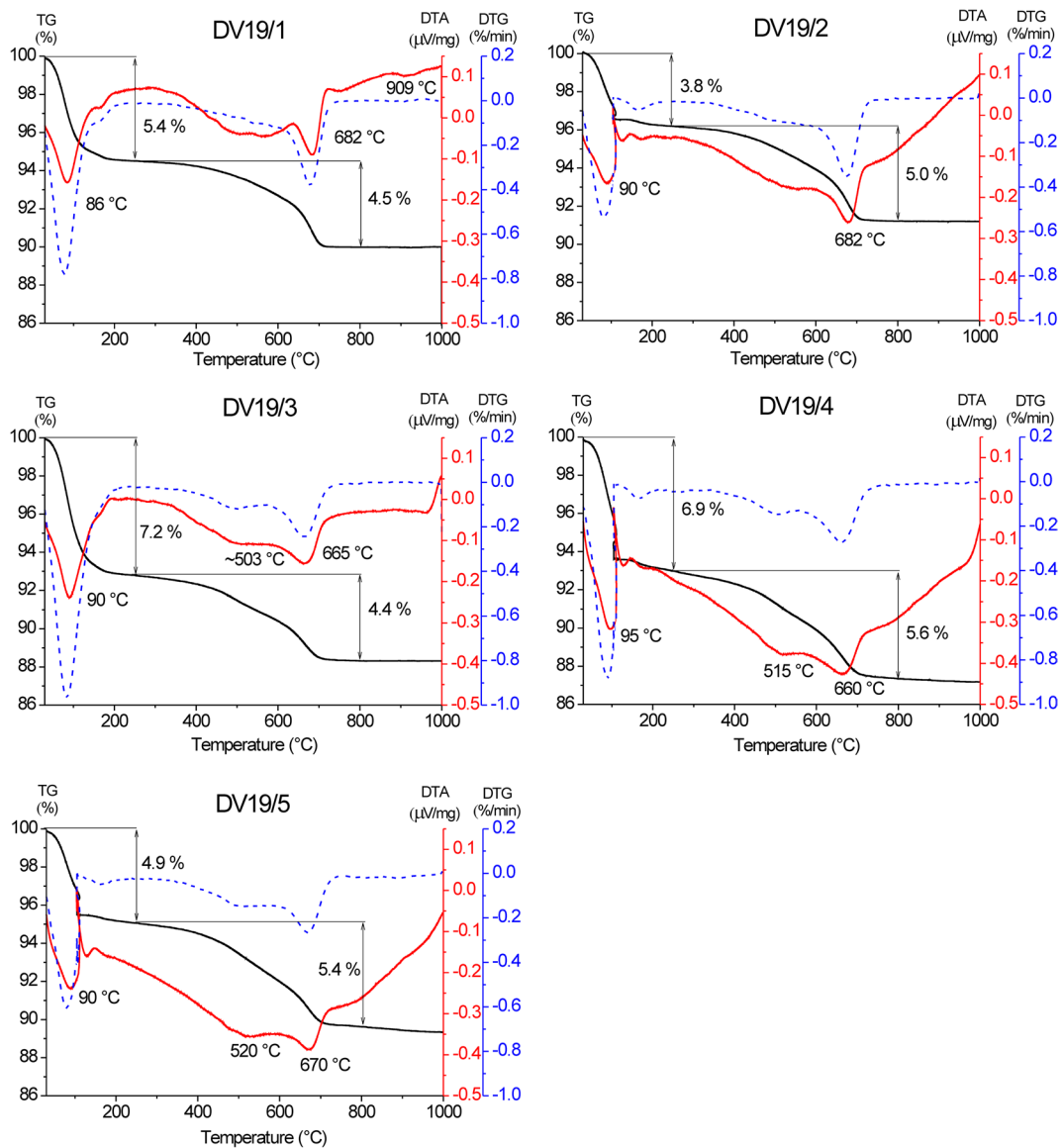


**Fig. 12** TG, DTG, and DTA curves of 0.2–2 μm fractions for K-bentonites

along with the elevated proportion of *tv* layers. The results from this limited data set (four samples) suggested that the *cv* interstratification for the illite-smectites may increase with octahedral Al content. Such a conclusion would be in line with the published data for illite-smectites from the Appalachian basin, USA (McCarty & Reynolds, 1995).

## Conclusions

In the current study, the two main technological types (i.e. types I and II) of K-bentonites from the Dolná Ves deposit were examined. The results revealed that the technological types of K-bentonites differ not only in their illite-smectite content but also in the characteristics of the illite-smectites present.

The type I (high-grade) K-bentonites contained 88–91 wt.% of illite-smectite whereas the type II (low-grade) K-bentonites consisted of 37–63 wt.% of illite-smectite. Depending on the raw material quality, variable amounts of quartz (2–61 wt.%) and feldspars (K-feldspar and plagioclase) (1–7 wt.%) were also present in the bulk K-bentonites. For most of the samples, illite-smectite was the only clay mineral constituent.

Illite-smectites isolated from the type I K-bentonites displayed R1 ordering, greater expandability ( $S_{\text{XRD}} \sim 28\text{--}35\%$ ), greater octahedral Mg (0.31–0.39 Mg per  $\text{O}_{20}(\text{OH})_4$ ), and less octahedral Fe (0.11–0.18 Fe per  $\text{O}_{20}(\text{OH})_4$ ) contents, smaller mean thickness of fundamental particles (2.4–2.8 nm), and a smaller number of 2:1 layers (three-layers) in the illite-smectite crystals. On the other hand, illite-smectites from the type II K-bentonites had  $R > 1$  ordering, less expandability ( $S_{\text{XRD}} \approx 10\text{--}22\%$ ), greater octahedral Fe (0.26–0.28 Fe per  $\text{O}_{20}(\text{OH})_4$ ) and less octahedral Mg (0.08–0.14 Mg per  $\text{O}_{20}(\text{OH})_4$ ), greater mean thickness of fundamental particles (2.9–4 nm), and a larger number of 2:1 layers (five- and six-layers) in illite-smectite crystals.

Significant correlations ( $p < 0.05$ ) were established between the quantitative mineral composition and chemical analysis, showing greater illite-smectite content in K-bentonites with increasing LOI (loss-on-ignition) and  $\text{Al}_2\text{O}_3$  content. Significant positive correlations were also found among the illite-smectite contents, expandability ( $S_{\text{XRD}}$ ), and CEC, indicating that the amount of illite-smectite and  $S_{\text{XRD}}$  had significant impact on CEC values.

Due to the greater expandability of illite-smectite, the type I K-bentonites displayed a much greater mass loss at  $< 250^\circ\text{C}$  (6.9–7.2%) than the type II K-bentonites (mass loss of 3.8–5.4%). The proportion of *cis*-vacant layers was greater for the type II K-bentonites whereas for the type I K-bentonites the proportion of *cis*-vacant layers was smaller, along with an elevated proportion of *trans*-vacant layers. The results suggested that the *cis*-vacant interstratification in illite-smectites may increase with greater octahedral Al content. Special clay ISCz-1 illite-smectite had properties similar to the type I K-bentonite. The physico-chemical properties indicated that the type I K-bentonites could be used in the ceramics, pharmaceutical, cosmetics, and food industries.

**Acknowledgements** The authors are grateful to Dr E. Puškelová (Slovak Academy of Sciences) for XRD measurements. The Editor-in-Chief, Associate Editor, and three reviewers are acknowledged for their constructive comments.

**Funding** Open access funding provided by The Ministry of Education, Science, Research and Sport of the Slovak Republic in cooperation with Centre for Scientific and Technical Information of the Slovak Republic This work was supported by the Slovak Research and Development Agency (APVV-20-0175), Slovak Grant Agency VEGA (1/0306/23) and the Ministry of Education, Science, Research and Sport of the Slovak Republic cofounded by the ERDF (Contract No. ITMS 26240220086).

**Data Availability** The data that support the findings of this study are available from the corresponding author, Marek OSACKÝ, upon reasonable request.

## Declarations

**Conflict of Interest** On behalf of all authors, the corresponding author states that there is no conflict of interest.

**Open Access** This article is licensed under a Creative Commons Attribution 4.0 International License, which permits use, sharing, adaptation, distribution and reproduction in any medium or format, as long as you give appropriate credit to the original author(s) and the source, provide a link to the Creative Commons licence, and indicate if changes were made. The images or other third party material in this article are included in the article's Creative Commons licence, unless indicated otherwise in a credit line to the material. If material is not included in the article's Creative Commons licence and your intended use is not permitted by statutory regulation or exceeds the permitted use, you will need to obtain permission directly from the copyright holder. To view a copy of this licence, visit <http://creativecommons.org/licenses/by/4.0/>.

## References

- Allo, W. A., & Murray, H. H. (2004). Mineralogy, chemistry and potential applications of a white bentonite in San Juan province, Argentina. *Applied Clay Science*, 25, 237–243. <https://doi.org/10.1016/j.clay.2003.10.003>
- Azzi, A. A., Osacký, M., Uhlík, P., Čaplovičová, M., Zanardo, A., & Madejová, J. (2016). Characterization of clays from Corumbataí formation used as raw material for ceramic industry in the Santa Gertrudes district, São Paulo, Brazil. *Applied Clay Science*, 132–133, 232–242. <https://doi.org/10.1016/j.clay.2016.06.009>
- Bain, D. C., & Smith, B. F. L. (1994). Chemical analysis. In M. J. Wilson (Ed.), *Clay Mineralogy: Spectroscopic and Chemical Determinative Methods* (pp. 300–322). Chapman & Hall.
- Čičel, B., & Komadel, P. (1994). Structural formulae of layer silicates. In James E. Amonette & Joseph W. Stucki (eds), *Quantitative Methods in Soil Mineralogy* (pp. 114–136). Chapter 4, Soil Science Society of America, Inc.
- Chernyshev, I. V., Haber, M., Kovalenker, V. A., Ivanenko, V. V., Jeleň, S., & Karpenko, M. I. (1995). The age of the magmatic events and epithermal Au-Ag-base metals mineralization in the central zone of the Banská Štiavnica stratovolcano: K/Ar data. *Geologica Carpathica*, 46(6), 327–334.
- Chernyshev, I. V., Konečný, V., Lexa, J., Kovalenker, V. A., Jeleň, S., Lebedev, V. A., & Goltsman, Y. V. (2013). K-Ar and Rb-Sr geochronology and evolution of the Štiavnica Stratovolcano (Central Slovakia). *Geologica Carpathica*, 64(4), 327–351. <https://doi.org/10.2478/geoca-2013-0023>
- Christidis, G. E., & Scott, P. W. (1997). The origin and control of colour of white bentonites from the Aegean Islands of Milos and Kimolos, Greece. *Mineralium Deposita*, 32, 271–279. <https://doi.org/10.1007/s001260050092>
- Demko, R., Lexa, J., Koděra, P., Biroň, A., Smolka, J., Šesták, P., Konečný, P., Tuček, L., Ferenc, Š., Bačo, P., Repčiak, M., Kollárová, V., Kyška-Pipík, R., Mikušová, J., Kotulová, J., B. G., & Vlachovič, J. (2010). Maps of Paleovolcanic Reconstruction of Slovak Rhyolite Volcanics and Analysis of Magmatic and Hydrothermal Processes. Open file report, ŠGÚDŠ, Bratislava, pp. 1–728 (in Slovak).
- Drits, V. A., Besson, G., & Muller, F. (1995). An improved model for structural transformations of heat-treated aluminum dioctahedral 2: 1 layer silicates. *Clays and Clay Minerals*, 43(6), 718–731. <https://doi.org/10.1346/CCMN.1995.0430608>
- Drits, V. A., Eberl, D. D., & Šrodoň, J. (1998). XRD measurement of mean thickness, thickness distribution and strain for illite and illite-smectite crystallites by the Bertaut-Warren-Averbach technique. *Clays and Clay Minerals*, 46(1), 38–50. <https://doi.org/10.1346/CCMN.1998.0460105>
- Drits, V. A., Lindgreen, H., & Salyn, A. L. (1997). Determination of the content and distribution of fixed ammonium in illite-smectite by x-ray diffraction: Application to North Sea illite-smectite. *American Mineralogist*, 82(1–2), 79–87. <https://doi.org/10.2138/am-1997-1-210>
- Drits, V. A., Salyn, A. L., & Šucha, V. (1996). Structural transformations of interstratified illite-smectites from Dolná Ves hydrothermal deposits: Dynamics and mechanisms. *Clays and Clay Minerals*, 44(2), 181–190. <https://doi.org/10.1346/CCMN.1996.0440203>
- Dudek, T., & Šrodoň, J. (1996). Identification of illite/smectite by X-ray powder diffraction taking into account the log-normal distribution of crystal thickness. *Geologica Carpathica Clays*, 5(1), 21–32.
- Dudek, T., Šrodoň, J., Eberl, D. D., Elsass, F., & Uhlík, P. (2002). Thickness distribution of illite crystals in shales. I: X-ray diffraction vs. high-resolution transmission electron microscopy measurements. *Clays and Clay Minerals*, 50(5), 562–577. <https://doi.org/10.1346/000986002320679305>
- Eberl, D. D. (2003). User's Guide to Rockjock—A Program for Determining Quantitative Mineralogy from Powder X-Ray Diffraction Data. U.S. Geological Survey Open-File Report 03–78, pp. 1–47. <https://pubs.usgs.gov/of/2003/of03-078/pdf/RockMan7.pdf>. Accessed 10 November 2023.
- Eberl, D. D., & Šrodoň, J. (1988). Ostwald ripening and interparticle-diffraction effects for illite crystals. *American Mineralogist*, 73, 1335–1345.
- Eberl, D. D., Drits, V. A., Šrodoň, J., & Nüesch, R. (1996). Mudmaster: A program for calculating crystallite size distributions and strain from the shapes of x-ray diffraction peaks. U.S. Geological Survey Open-File Report 96–171, pp. 1–57. <https://pubs.usgs.gov/of/1996/of96-171/pdf/MudMan.pdf>. Accessed 10 November 2023.
- Eberl, D. D., Nüesch, R., Šucha, V., & Tsipursky, S. (1998). Measurement of fundamental illite particle thicknesses by X-ray diffraction using PVP-10 intercalation. *Clays and Clay Minerals*, 46(1), 89–97. <https://doi.org/10.1346/CCMN.1998.0460110>
- Elsass, F., Beaumont, A., Pernes, M., Jaunet, A., & Tessier, D. (1998). Changes in layer organization of Na- and Ca-exchange smectite materials during solvent exchanges for embedment in resin. *The Canadian Mineralogist*, 36, 1475–1483.
- Farmer, V. C. (1974). The layer silicates. In Farmer V. C. (Eds) *Infrared spectra of minerals*. Mineral Society, pp. 331–363.
- Geramian, M., Osacký, M., Ivey, D. G., Liu, Q., & Etsell, T. H. (2016). Effect of swelling clay minerals (montmorillonite and illite-smectite) on nonaqueous bitumen extraction from Alberta oil sands. *Energy & Fuels*, 30, 8083–8090. <https://doi.org/10.1021/acs.energyfuels.6b01026>
- Górniak, K., Szydłak, T., Gawel, A., Klimek, A., Tomczyk, A., Motyka, J., & Bahranowski, B. (2017). Smectite-, silica- and zeolite-bearing raw materials (Hliník nad Hronom bentonite, Slovakia) — A new approach using integrated petrographic and mineralogical studies. *Applied Clay Science*, 141, 180–191. <https://doi.org/10.1016/j.clay.2017.02.032>
- Górniak, K., Szydłak, T., Gawel, A., Klimek, A., Tomczyk, A., Sulikowski, B., Olejniczak, Z., Motyka, J., Serwicka, E. M., & Bahranowski, B. (2016). Commercial bentonite from the Kopernica deposit (Tertiary, Slovakia): A petrographic and mineralogical approach. *Clay Minerals*, 51(1), 97–122. <https://doi.org/10.1180/claymin.2016.051.1.09>
- Hower, J., Eslinger, E. V., Hower, M. E., & Perry, E. A. (1976). Mechanism of burial metamorphism of argillaceous sediment: 1. Mineralogical and chemical evidence. *Geological Society of America Bulletin*, 87, 725–737. [https://doi.org/10.1130/0016-7606\(1976\)87%3c725:MOBMOA%3e2.0.CO;2](https://doi.org/10.1130/0016-7606(1976)87%3c725:MOBMOA%3e2.0.CO;2)
- Hroncová, Z., Sýkora, J., Adamják, M., & Viest, L. (1992). Final report Dolná Ves—preliminary survey, ceramic raw materials. Geologický prieskum, š.p. Spišská Nová Ves, pp. 1–117 (in Slovak).

- Inoue, A., Lanson, B., Marques-Fernandes, M., Sakharov, B. A., Murakami, T., Meunier, A., & Beaufort, D. (2005). Illite-smectite mixed-layer minerals in the hydrothermal alteration of volcanic rocks: I. One-dimensional XRD structure analysis and characterization of component layers. *Clays and Clay Minerals*, 53(5), 423–439. <https://doi.org/10.1346/CCMN.2005.0530501>
- Inoue, A., Minato, H., & Utada, M. (1978). Mineralogical properties and occurrence of illite/montmorillonite mixed layer minerals formed from Miocene volcanic glass in Waga-Omono district. *Clay Science*, 5, 123–136. <https://doi.org/10.11362/jcssjclayscience1960.5.123>
- Jagodzinski, H. (1949). Eindimensionale fehlordnung in kristallen und ihr einfluss auf die Röntgeninterferenzen. I. Berechnung des fehlordnungsgrades an der Röntgenintensitäten. *Acta Crystallographica*, 2, 201–207.
- Koděra, P., Lexa, J., Fallick, A. E., Wälle, M., & Biroň, A. (2014). Hydrothermal fluids in epithermal and porphyry Au deposits in the Central Slovakia volcanic field. *Geological Society Special Publication*, 402(1), 177–206. <https://doi.org/10.1144/sp402.5>
- Konečný, V., Lexa, J., & Planderová, E. (1983). Stratigraphy of the Central Slovakia volcanic field. *Západné Karpaty. Sér. Geol.*, 9, 1–203. (in Slovak with English summary).
- Kraus, I., Šamajová, E., Šucha, V., Lexa, J., & Hroncová, Z. (1994). Diagenetic and hydrothermal alterations of volcanic rocks into clay minerals and zeolites (Kremnické Vrchy Mountains, Western Carpathians). *Geologica Carpathica*, 45(3), 151–158.
- Lexa, J., & Konečný, V. (1998). Geodynamic aspects of the Neogene to Quaternary volcanism. In: Rakús, M. (Ed.) *Geodynamic Development of the Western Carpathians*. GSSR, pp. 219–240.
- Lexa, J., & Pécskay, Z. (2010). Radiometric dating of rhyolites by conventional K/Ar method: methodical aspects. In: Kohút, M. (Ed.) *Dating of Minerals and Rocks, Metamorphic, Magmatic and Metallogenic Processes, as Well as Tectonic Events*. ŠGÚDŠ, pp. 21–22.
- Lexa, J., Halouzka, R., Havrila, M., Hanzel, V., Kubeš, P., Liščák, P., & Hojstričová, V. (1998). Explanatory notes to the geological map of Kremnické vrchy mountain range. Geological Survey of Slovak Republic, pp. 1–308 (in Slovak).
- Lexa, J., Varga, P., Uhlík, P., Koděra, P., Biroň, A., & Rajnoha, M. (2021). Perlite deposits of the Central Slovakia Volcanic Field (Western Carpathians): Geology and properties. *Geologica Carpathica*, 72(3), 253–281. <https://doi.org/10.31577/GeolCarp.72.3.5>
- Madejová, J., & Komadel, P. (2001). Baseline studies of the clay minerals society source clays: Infrared methods. *Clays and Clay Minerals*, 49(5), 410–432. <https://doi.org/10.1346/CCMN.2001.0490508>
- McCarty, D. K., & Reynolds, R. C., Jr. (1995). Rotationally disordered illite/smectite in Paleozoic K-bentonites. *Clays and Clay Minerals*, 43(3), 271–284. <https://doi.org/10.1346/CCMN.1995.0430302>
- Meier, L. P., & Kahr, G. (1999). Determination of the cation exchange capacity (CEC) of clay minerals using the complexes of copper(II) ion with triethylenetetramine and tetraethylenepentamine. *Clays and Clay Minerals*, 47(3), 386–388. <https://doi.org/10.1346/CCMN.1999.0470315>
- Moore, D.M., & Reynolds Jr, R.C. (1997). *X-ray diffraction and the identification and analysis of clay minerals*. 2<sup>nd</sup> ed. Oxford University Press.
- Muller, F., Drits, V., Plançon, A., & Robert, J.-L. (2000). Structural transformation of 2:1 dioctahedral layer silicates during dehydroxylation-rehydroxylation reactions. *Clays and Clay Minerals*, 48(5), 572–585. <https://doi.org/10.1346/CCMN.2000.0480510>
- Omotoso, O., & Eberl, D. D. (2009). Sample preparation and data collection strategies for X-ray diffraction quantitative phase analysis of clay-bearing rocks. 46th Annual Meeting of the Clay Minerals Society, June 5–11 2009, Billings, Montana, USA, p. 209.
- Osacký, M., Binčík, T., Paľo, T., Uhlík, P., Madejová, J., & Czímerová, A. (2019). Mineralogical and physico-chemical properties of bentonites from the Jastrabá Formation (Kremnické vrchy Mts., Western Carpathians). *Geologica Carpathica*, 70(5), 433–445. <https://doi.org/10.2478/geoca-2019-0025>
- Pécskay, Z., Molnár, F., Itaya, T., & Zelenka, T. (2005). Geology and K-Ar geochronology of illite from the clay deposit at Füzérradvány, Tokaj Mt., Hungary. *Acta Mineralogica Petrographica*, 46, 1–7.
- Pentrák, M., Czímerová, A., Madejová, J., & Komadel, P. (2012). Changes in layer charge of clay minerals upon acid treatment as obtained from their interactions with methylene blue. *Applied Clay Science*, 55, 100–107. <https://doi.org/10.1016/j.clay.2011.10.012>
- Šrodoň, J. (1980). Precise identification of illite/smectite interstratifications by X-ray powder diffraction. *Clays and Clay Minerals*, 28(6), 401–411. <https://doi.org/10.1346/CCMN.1980.0280601>
- Šrodoň, J. (1999). Nature of mixed-layer clays and mechanisms of their formation and alteration. *Annual Review of Earth and Planetary Sciences*, 27, 19–53. <https://doi.org/10.1146/annurev.earth.27.1.19>
- Šrodoň, J., Andreoli, C., Elsass, F., & Robert, M. (1990). Direct high-resolution transmission electron microscopic measurement of expandability of mixed-layer illite/smectite in bentonite rock. *Clays and Clay Minerals*, 38(4), 373–379. <https://doi.org/10.1346/CCMN.1990.0380406>
- Šrodoň, J., Drits, V. A., McCarty, D. K., Hsieh, J. C. C., & Eberl, D. D. (2001). Quantitative X-ray diffraction analysis of clay-bearing rocks from random preparations. *Clays and Clay Minerals*, 49(6), 514–528. <https://doi.org/10.1346/CCMN.2001.0490604>
- Šrodoň, J., Elsass, F., McHardy, W. J., & Morgan, D. J. (1992). Chemistry of illite-smectite inferred from TEM measurement of fundamental particles. *Clay Minerals*, 27, 137–158. <https://doi.org/10.1180/claymin.1992.027.2.01>
- Šamajová, E., Kraus, I., & Lajčáková, A. (1992). Diagenetic alteration of Miocene acidic vitric tuffs of the Jastrabá Formation (Kremnické vrchy Mts., Western Carpathians). *Geologica Carpathica*, 1(1), 21–26.
- Šoltés, S., Kúšik, D., Mižák, J., & Kubač, A. (2021). Slovak Minerals Yearbook 2020. ŠGÚDŠ, Bratislava, 143 pp.
- Šucha, V., Kraus, I., Mosser, C., Hroncová, Z., Soboleva, K. A., & Siranova, V. (1992). Mixed-layer illite/smectite from the Dolná Ves hydrothermal deposit, the Western Carpathians Kremnica Mts. *Geologica Carpathica*, 1(1), 13–19.

- Šucha, V., Šrodoň, J., Clauer, N., Elsass, F., Eberl, D. D., Kraus, I., & Madejová, J. (2001). Weathering of smectite and illite-smectite under temperate climatic conditions. *Clay Minerals*, 36(3), 403–419. <https://doi.org/10.1180/000985501750539490>
- Šucha, V., Šrodoň, J., Elsass, F., & McHardy, W. J. (1996). Particle shape versus coherent scattering domain of illite/smectite: Evidence from HRTEM of Dolna Ves clays. *Clays and Clay Minerals*, 44(5), 665–671. <https://doi.org/10.1346/CCMN.1996.0440509>
- Tessier, D. (1984). *Étude expérimentale de l'organisation des matériaux argileux*. University of Paris VII.
- Uhlík, P., & Majzlan, J. (2004). Conditions of mixed-layer illite-smectite formation at the deposit Dolná Ves on the southwest margin of Kremnica stratovolcano. *Mineralia Slovaca*, 36, 331–338.
- Weaver, C. E. (1953). Mineralogy and petrology of some Ordovician K-bentonites and related limestones. *Bulletin of the Geological Society of America*, 64, 921–944. [https://doi.org/10.1130/0016-7606\(1953\)64\[921:MAPOSO\]2.0.CO;2](https://doi.org/10.1130/0016-7606(1953)64[921:MAPOSO]2.0.CO;2)
- Zuberec, J., Tréger, M., Lexa, J., & Baláž, P. (2005). Mineral resources of Slovakia. ŠGÚDŠ, pp. 1–320.